Energy Conversion and Management 150 (2017) 851–869

Contents lists available at ScienceDirect

Energy Conversion and Management

journal homepage: www.elsevier.com/locate/enconman

Industrial waste-heat recovery through integrated computer-aided working-fluid and ORC system optimisation using SAFT-γ Mie

Martin T. White, Oyeniyi A. Oyewunmi, Andrew J. Haslam, Christos N. Markides *

Clean Energy Processes (CEP) Laboratory, Department of Chemical Engineering, Imperial College London, South Kensington Campus, London SW7 2AZ, UK

ARTICLE INFO

Article history:
Available online 25 April 2017

Keywords:
ORC
Waste-heat recovery
CAMD
Working fluid
Optimisation
SAFT
Group contribution

ABSTRACT

A mixed-integer non-linear programming optimisation framework is formulated and developed that combines a molecular-based, group-contribution equation of state, SAFT-γ Mie, with a thermodynamic description of an organic Rankine cycle (ORC) power system. In this framework, a set of working fluids is described by its constituent functional groups (*e.g.*, since we are focussing here on hydrocarbons: —CH_3, —CH_2—, *etc.*), and integer optimisation variables are introduced in the description the working-fluid structure. Molecular feasibility constraints are then defined to ensure all feasible working-fluid candidates can be found. This optimisation framework facilitates combining the computer-aided molecular design of the working fluid with the power-system optimisation into a single framework, thus removing subjective and pre-emptive screening criteria, and simultaneously moving towards the next generation of tailored working fluids and optimised systems for waste-heat recovery applications. SAFT-γ Mie has not been previously employed in such a framework. The optimisation framework, which is based here on hydrocarbon functional groups, is first validated against an alternative formulation that uses (pseudo-experimental) thermodynamic property predictions from REFPROP, and against an optimisation study taken from the literature. The framework is then applied to three industrial waste-heat recovery applications. It is found that simple molecules, such as propane and propene, are the optimal ORC working fluids for a low-grade (150 °C) heat source, whilst molecules with increasing molecular complexity are favoured at higher temperatures. Specifically, 2-alkenes emerge as the optimal working fluids for medium- and higher-grade heat-sources in the 250–350 °C temperature range. Ultimately, the results demonstrate the potential of this framework to drive the search for the next generation of ORC systems, and to provide meaningful insights into identifying the working fluids that represent the optimal choices for targeted applications. Finally, the effects of the working-fluid structure on the expander and pump are investigated, and the suitability of group-contribution methods for evaluating the transport properties of hydrocarbon working-fluids are considered, in the context of performing complete thermoeconomic evaluations of these systems.

1. Introduction

Increasing concerns over depleting fossil-fuel reserves and the detrimental effects on human health and the environment linked to the release of their combustion products have led to a surge of interest in renewable and sustainable energy systems in recent years. Within this remit fall a number of technologies which aim to recover waste heat from a variety of industrial processes, and which are of particular interest given their significant potential to improve resource utilisation efficiency and to reduce simultaneously industrial primary energy use and emissions. One such technology is the organic Rankine cycle (ORC), which is highly suitable for the conversion of lower-temperature (or, lower-grade) heat to useful electrical power, either for on-site use or export to the grid [1]. This ability to utilise effectively heat sources at lower temperatures is facilitated by the lower critical temperatures of organic working-fluids, compared to using conventional Rankine cycles, for example. Typically, for heat sources with temperatures between 100 and 400 °C and at scales (in the power range) of a few kW up to tens of MW, the ORC can be considered a suitable technology for the conversion of heat to power with thermal efficiencies in excess of 25% reported at the higher temperatures and larger scales. Although ORC technology has achieved some maturity, with units available commercially from manufacturers and aimed at the aforementioned ranges of temperatures and sizes,

* Corresponding author.
E-mail address: c.markides@imperial.ac.uk (C.N. Markides).

http://dx.doi.org/10.1016/j.enconman.2017.03.048
0196-8904/

Nomenclature

Abbreviations

BWR	Back work ratio
CAMD	Computer-aided molecular design
MINLP	Mixed-integer non-linear programming
ORC	Organic Rankine cycle
SAFT	Statistical associating fluid theory
WHR	Waste heat recovery

Greek symbols

η	efficiency
η_L	liquid dynamic viscosity, Pa s
η_V	vapour dynamic viscosity, Pa s
λ_L	liquid thermal conductivity, W/(m K)
λ_V	vapour thermal conductivity, W/(m K)
ω	acentric factor
σ	surface tension, N/m

Roman symbols

ΔT_{sh}	degree of superheating, K
$\dot{m}$	mass flow rate, kg/s
$\dot{W}$	power, W
Ma	mach number
PP	pinch point, K
c_p	specific heat capacity at constant pressure, J/(kg K)
c_v	specific heat capacity at constant volume, J/(kg K)
h	specific enthalpy, J/kg
P	pressure, Pa
P_r	reduced pressure
T	temperature, K
T_r	reduced temperature
V_m	specific (molar) volume, m^3/mol
w	specific work, J/kg

Subscripts

1–4	ORC state points
b	boiling
c	heat sink
cr	critical point
e	expander
h	heat source
i	inlet
n	net
o	outlet
p	pinch, pump
th	thermal

a number of important challenges remain that limit the true potential of this technology, both from technical and economic perspectives [2].

Due to the large number of potential ORC working-fluids, working-fluid selection has remained a particular focus of research. First and foremost, thermodynamic performance remains one of the most important drivers, and there have been many studies concerning the thermodynamic analysis of ORC systems. Chen et al. [3] categorised working fluids based on critical temperature and the slopes of their saturation curves, with the aim of providing general selection criteria based on the heat-source temperature and cycle architecture. Alternatively, many parametric studies have been completed in which a number of working-fluids are optimised for the same heat-source conditions and an optimal working-fluid is selected based on thermodynamic performance, for example in Refs. [4–6]. More recently, Li et al. [7] identified optimal working-fluids for heat-source temperatures between 200 and 500 °C, whilst Song et al. [8] incorporated component modelling into the working-fluid selection procedure.

Alongside using pure working-fluids, it is also possible to consider using fluid mixtures. Lecompte et al. [9] report possible improvements in the second law efficiency between 7.1 and 14.2%, and similar improvements in thermodynamic performance have been reported in Refs. [10–12]. Furthermore, Zhou et al. [13] investigated working-fluid mixtures operating within partially evaporated ORC systems. Whilst many of these studies report higher power outputs and higher exergy efficiencies, they also report larger heat exchanger costs.

In addition to thermodynamic performance, more general working-fluid selection criteria are also available in the literature, and these consider aspects such as component performance, material compatibility, safety, environmental properties and cost. In an early study, Badr et al. [14] listed the desirable properties of a working fluid, and more recently, Rahbar et al. [15] reported similar selection criteria. Specific research into the thermal stability of working-fluids for high temperature waste heat recovery (WHR) has also been conducted [16]. In general, working-fluid selection criteria are introduced during a fluid-selection study in which a group of known fluids, taken from a database such as NIST [17], are screened based on predefined criteria. For example, Drescher and Brüggemann [18] evaluated 1,800 substances, from which five were identified as suitable working-fluids for a biomass application. Similiarly, Tchanche et al. [19] evaluated 20 fluids for a 90 °C heat source, and whilst no fluid met all selection criteria, optimal working-fluids were identified after a qualitative comparison was conducted. More recently, Schwöbel et al. [20] devised a screening process in which 3,174 fluids were considered for a particular application. However, after identifying an optimal working fluid from a thermodynamic perspective, it was necessary to reject this fluid due to safety concerns, highlighting the difficulty in identifying a fluid which meets all predefined criteria.

Alternatively, computer-aided molecular design (CAMD) could be used to identify optimal working-fluids. In CAMD several molecular groups are defined (*e.g.*, —CH_3, —CH_2—, >CH—, >C<, =CH_2, =CH—) which can be combined according to a series of rules in order to form different molecules. Initially, CAMD was applied to solvent design and used to identify molecules with specific solvent properties [21]. More recently, this has developed further and involves coupling CAMD methods with process models, facilitating the integrated design and optimisation of the solvent and the separation process [22–25]. Such problems require molecular feasibility constraints, a group-contribution equation of state, and a mixed-integer non-linear programming (MINLP) optimiser. Molecular feasibility constraints ensure a generated set of molecular groups is a genuine molecule [26–28], whilst a group-contribution equation of state determines the fluid properties of a molecule based on the molecular groups from which it is composed. Early examples are the empirical Joback and Reid group-contribution method [29] and the UNIFAC method [30]. However, an alternative to these empirical methods is the use of molecular-based equations of state based on statistical associating fluid theory (SAFT) [31,32], for which group-contribution methods have recently become available [33–44].

The application of CAMD to ORC problems allows the working fluid and thermodynamic system to be simultaneously optimised in a single CAMD-ORC optimisation framework. This framework

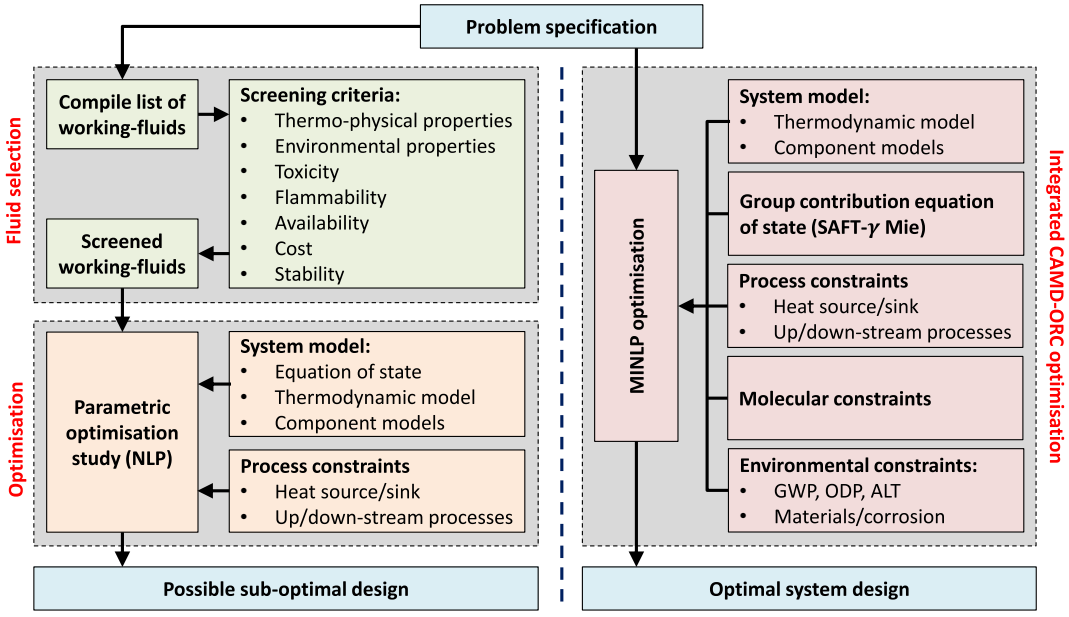

Fig. 1. Schematic of a conventional ORC optimisation study (left) and the integrated CAMD-ORC approach (right).

is compared to a conventional ORC optimisation study in Fig. 1. In the conventional optimisation study a large array of working fluids are evaluated based on predefined screening criteria. Then for each screened working fluid a system-level optimisation is completed and the optimal working fluid is selected by comparing the results of these individual optimisations. However, this method can lead to sub-optimal system designs since optimal working fluids could be excluded based on subjective screening criteria. By comparison, the CAMD-ORC approach could remove the screening criteria entirely.

Papadopoulos et al. [45] formulated a CAMD-ORC framework, paying particular attention to safety and environment characteristics of the working fluid, and later applied CAMD to the design and selection of mixtures for ORC systems [46]. Brignoli and Brown [47] developed an ORC model based on a cubic equation of state, and coupled this to group-contribution methods. This allowed a parametric investigation into the effect of the critical point parameters on the ORC performance, and it was suggested that this method could be used to identify new working-fluids in the future. Palma-Flores et al. [48] formulated a CAMD-ORC framework for WHR applications and found that through CAMD it is possible to both improve the thermal efficency of the system and the safety characteristics of the working fluid. Another recent study, conducted by Su and Deng [49], also employed group-contribution methods within an ORC model. A comparison with REFPROP identified deviations in ORC thermodynamic parameters of less than 10%, and the authors plan on implementing the model within a CAMD-ORC framework in the future.

Until now, the CAMD-ORC studies discussed rely on empirical group-contribution methods. Alternatively, a particular version of SAFT, PC-SAFT [50,51], has been applied within a CAMD-ORC framework. Lampe et al. [52,53] used PC-SAFT to optimise an ORC system for a geothermal application, and did so by splitting the optimisation process into two-stages. In the first stage a hypothetical optimum working-fluid is identified, whilst in the second stage real working-fluids are identified that exhibit similar performance to the hypothetical optimum. More recently, Schilling et al. [54] integrated PC-SAFT with a process model of the ORC system, and conducted a single-stage optimisation. The model was applied to a WHR case study and the results identified both the most promising working fluids from existing working-fluid databases, in addition to generating novel molecular structures. However, the main focus of this study was on optimising the thermodynamic performance of the system.

Previously, Oyewunmi et al. [12] evaluated an alternative formulation of SAFT, SAFT-VR Mie [55], to optimise working-fluid mixtures for ORC systems. The group-contribution counterpart, SAFT-γ Mie [44], has been shown to provide a good description of fluid-phase thermodynamic properties of *n*-alkanes and a variety of other fluids; in particular, calculated saturation properties exhibit good agreement with experimental or pseudo-experimental data [17,44,56–58]. The aim of this paper is to formulate a CAMD-ORC framework using SAFT-γ Mie and to apply this to industrially relevant WHR applications. This study is the first to use SAFT-γ Mie within this context, and the results obtained not only identify optimal working-fluids, but also contribute important information regarding the characteristics that an optimal working-fluid should possess. Furthermore, this paper is also the first study to evaluate group-contribution methods for determining transport properties. These results will inform future modelling efforts, allowing heat exchanger sizing models and cost correlations to be integrated into the CAMD-ORC framework. This, in turn, facilitates techno-economic optimisations to be completed, allowing the CAMD-ORC framework to move beyond previous CAMD-ORC studies focussed on thermodynamic performance.

In Section 2, we describe the CAMD-ORC framework, before completing several validation studies in Section 3. In Section 4, the CAMD-ORC framework is used to investigate the optimal design of hydrocarbon working fluids for three different heat-source temperatures. Finally, in Section 5, an expander model is introduced, and group-contribution methods for determining transport properties are evaluated.

2. Model description

The full CAMD-ORC MINLP optimisation problem is solved in the gPROMS modelling environment [59], and consists of four components. These are the SAFT-γ Mie group-contribution equation of state, molecular constraints, the ORC process model and the MINLP optimisation algorithm. A schematic of this model was shown in Fig. 1.

2.1. SAFT-γ Mie equation of state

A group-contribution equation of state predicts the thermodynamic properties of a working fluid based on the molecular groups from which it is composed. Examples of molecular groups relevant to this work are single-bonded hydrocarbon groups such as —CH_3, —CH_2—, >CH—, >C<, and double-bonded hydrocarbon groups such as =CH_2, =CH— and =C<, which can be used to construct a wide range of alkane and alkene working fluids. Group-contribution methods have been available for decades [29]. However, these methods only provide important parameters such as the critical temperature and critical pressure, rather than providing all of the thermodynamic properties required to evaluate a thermodynamic system. Instead, this work makes use of the SAFT-γ Mie group-contribution equation of state.

Statistical associating fluid theory (SAFT) equations of state have a foundation in statistical mechanics, which gives them a predictive capability not seen in other equations of state that rely on experimental data. In SAFT, a working fluid is modelled as a chain of spherical segments, and the Helmholtz free energy is determined by as sum of individual ideal and residual contributions; the latter are decomposed into monomer, chain and association terms. Then, from the Helmholtz free energy, all thermodynamic properties of interest can be determined. In SAFT-γ Mie the interaction between two molecular groups is described by a Mie potential [44], and currently SAFT-γ Mie parameters are available for a variety of molecular groups [56], including the hydrocarbon groups mentioned previously.

2.2. Molecularly feasibility constraints

In constructing a molecule from molecular groups, rules of stoichiometry and valence must be obeyed. To ensure that a generated set of molecular groups represents a genuine molecule it is therefore necessary to introduce molecular feasibility constraints. In this study, non-cyclic molecules of single and double-bonded hydrocarbon groups are considered. The first constraint ensures that all free attachments of a group are occupied in a bond. This implies:

$$\sum_{\mathrm{i}} n_{\mathrm{i}} = \frac{1}{2}\sum_{\mathrm{j}} n_{\mathrm{j}} v_{\mathrm{j}} + 1, \tag{1}$$

where n_{i} is number of group i present, and v_{i} is the valency of group i that is defined as the number of other groups to which that group can attach; *e.g.*, the valency of both —CH_3 and =CH_2 is one, whilst the valency of —CH_2— and =CH— is two and so on. It is also required that each group with a double bond has another double bond to which it can attach, hence:

$$\sum_{\mathrm{i}} n_{\mathrm{i}} d_{\mathrm{i}} = 2j \quad \text{where } j = \{0, 1, 2, \ldots\}, \tag{2}$$

where $d_{\mathrm{i}} = 1$ if group i contains a double bond, and $d_{\mathrm{i}} = 0$ otherwise.

In addition to this, the number of groups linked by only one double bond (*i.e.*, =CH_2) must be less than or equal to the number of groups linked by one double bond and additional single bonds (*i.e.*, =CH—). In addition to the constraints listed here, molecular constraints for triple-bonded and cyclic molecules have also been developed and implemented within the CAMD-ORC model. These constraints will become important in future studies when the analysis presented in this paper is extended to include the groups that make up these molecules.

2.3. ORC model

The ORC system is defined as a single-stage, subcritical, non-recuperated cycle. A schematic and *T-s* diagram of this cycle is shown in Fig. 2 in which the notation used within this paper is defined.

The performance of this system is a function of three system variables: the condensation temperature T_1; the reduced pressure $P_{\mathrm{r}} = P_2/P_{\mathrm{cr}}$, where P_{cr} is the critical pressure; and the amount of superheat ΔT_{sh}. The pump and expansion processes are modelled by specified isentropic efficiencies, denoted η_{p} and η_{t} respectively, which enables the pump specific work w_{p} and expander specific work w_{e} to be determined. This fully defines all of the cycle state points, from which the net specific work w_{n} and thermal efficiency η_{th} follow:

$$w_{\mathrm{n}} = w_{\mathrm{e}} - w_{\mathrm{p}} = (h_3 - h_4) - (h_2 - h_1); \tag{3}$$

$$\eta_{\mathrm{th}} = \frac{w_n}{h_3 - h_2}. \tag{4}$$

The heat source is defined by an inlet temperature T_{hi}, mass flow rate $\dot{m}_{\mathrm{h}}$ and specific heat capacity $c_{\mathrm{p,h}}$. The amount of heat transferred from the heat source to the working fluid is then modelled by applying an energy balance. The evaporator pinch point PP_{h} is defined, as a model input, as the temperature between the heat source and working fluid at the beginning of evaporation (*i.e.*, $PP_{\mathrm{h}} = T_{\mathrm{hp}} - T_{2'}$). The working-fluid mass flow rate is given by:

$$\dot{m}_{\mathrm{o}} = \frac{\dot{m}_{\mathrm{h}} c_{\mathrm{p,h}} (T_{\mathrm{hi}} - T_{\mathrm{hp}})}{h_3 - h_{2'}}. \tag{5}$$

The net power output from the system is then given by $\dot{W}_{\mathrm{n}} = \dot{m}_{\mathrm{o}} w_{\mathrm{n}}$. The heat sink is also defined by an inlet temperature T_{ci}, mass flow rate $\dot{m}_{\mathrm{c}}$ and specific heat capacity $c_{\mathrm{p,c}}$. By applying

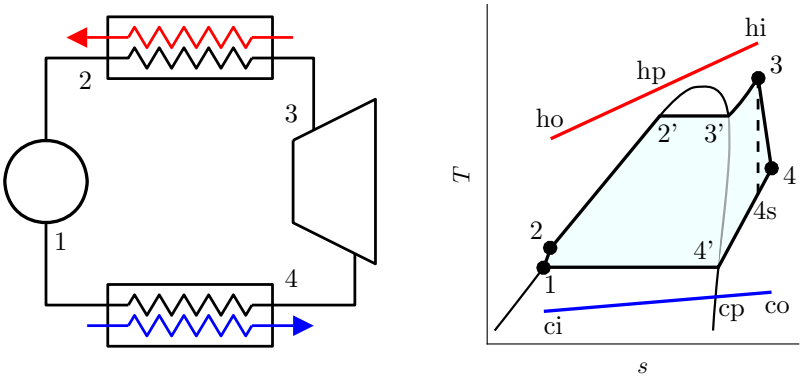

Fig. 2. A schematic of the ORC system and the notation used to describe it.

another energy balance to the condenser, the condenser pinch point, PP_c, is determined, and this must be greater than the minimum allowable pinch point $PP_{c,min}$:

$$PP_c = T_{4'} - \left(T_{ci} + \frac{\dot{m}_o(h_{4'} - h_1)}{\dot{m}_c c_{p,c}}\right) \geqslant PP_{c,min}. \quad (6)$$

Whilst the condensation pressure is controlled by the condensation temperature, the evaporation pressure is controlled by the input reduced pressure P_r. The use of the P_r, rather than directly specifying P_2, ensures the cycle remains within the subcritical operating regime regardless of the working fluid, and this ensures a more numerically stable optimisation. However, when using the SAFT-γ Mie equation of state within gPROMS there is currently no supported method for determining the critical properties. Instead, the critical point can be determined manually by constructing the vapour-pressure curve. Therefore it is necessary to implement an alternative method. In this paper, the Joback and Reid group-contribution method [29] is used, which determines the critical pressure of a working-fluid:

$$P_{cr} = \left(a + bn_A - \sum_i P_{cr,i}\right)^{-2}, \quad (7)$$

where $a = 0.113$, $b = 0.0032$, n_A is the total number of atoms in the molecule, and $P_{cr,i}$ is the individual contribution from each group i. The contributions for each group considered within this paper can be found in Ref. [29].

The predictions made using the Joback and Reid method have been compared to NIST data for the alkane and alkene working fluids available in the NIST database. Furthermore, the critical pressures of these working fluids have also been obtained manually using SAFT-γ Mie. The results from this analysis are shown in Fig. 3.

From Fig. 3 it is observed that for all the fluids considered the Joback and Reid method agrees with the NIST data to within ±10%, thus confirming that the Joback and Reid is sufficiently accurate to determine the critical pressure of alkane and alkene working fluids. The difference between SAFT-γ Mie and NIST is greater, with SAFT-γ Mie, on average, over predicting the critical pressure by 10%. However, this is not considered a problem since SAFT-γ Mie over predicting the critical pressure actually helps the numerical stability of the optimisation process. For example, if a maximum limit of $P_r = 0.85$ is applied during an optimisation and P_{cr} is obtained using the Joback and Reid method, the resulting maximum pressure will be lower than the critical pressure predicted by SAFT-γ Mie, thus ensuring the calculation will not fail.

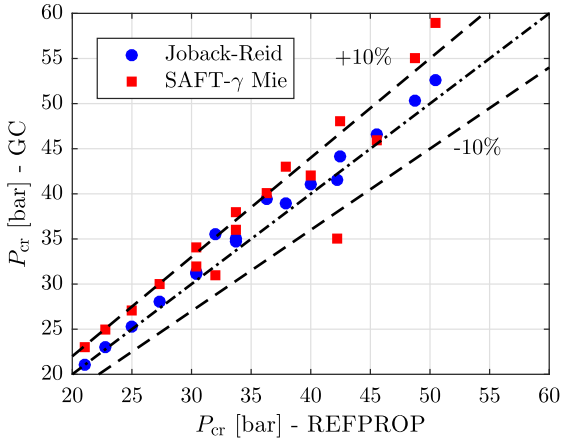

Fig. 3. A comparison between the critical pressures obtained using Joback and Reid, SAFT-γ Mie and NIST REFPROP for the alkane and alkene working-fluids available in NIST REFPROP.

2.4. Optimisation problem definition

In this work the aim of the optimisation is to determine the optimal combination of the molecular groups and thermodynamic variables that maximise the power output generated by the ORC for a specified heat source and heat sink. The optimisation problem consists of integer optimisation variables describing the working-fluid, and continuous variables describing the thermodynamic system, and therefore the whole problem is a mixed-integer non-linear programming (MINLP) problem. Mathematically, the optimisation setup can be described as:

$$\max \{\dot{W}_n(x,y)\}, \quad (8)$$

subject to:

$$g(x,y) \leqslant 0; \quad (9)$$

$$h(x,y) \leqslant 0; \quad (10)$$

$$x_{min} \leqslant x \leqslant x_{max}; \quad (11)$$

$$y_{min} \leqslant y \leqslant y_{max}; \quad (12)$$

where x and y are vectors containing the ORC system variables and the working-fluid variables respectively, $g(x,y)$ are the process model constraints and $h(x,y)$ are the molecular constraints. Inequalities (11) and (12) represent the lower and upper bounds for the optimisation variables.

Within gPROMS the OAERAP [59] solver is used; this employs an outer approximation algorithm to solve MINLP optimisation problems. Firstly, all discrete variables are relaxed such that they can take any continuous value between the defined lower and upper bounds, and a non-linear programming (NLP) optimisation is completed. This supplies a maximum value for objective function, and the corresponding optimal values for the decision variables. In the second step, the objective function and constraints are linearised and a mixed-integer linear programming (MILP) problem is solved to determine optimal values for the continuous and the discrete variables. Based on the optimal point found by the MILP optimisation, the discrete decision variables describing the working fluid are fixed, and the continuous variables that describe the thermodynamic cycle are optimised further (NLP). If the result from this NLP optimisation is feasible, the current values for the decision variables and objective function are stored, before the algorithm moves onto another iteration in which the MILP and NLP optimisation stages are repeated. This process repeats until the change in the objective function is less than the convergence tolerance, or until the maximum number of iterations has been reached.

3. Model validation

3.1. Validation of the molecular constraints

To validate the molecular feasibility constraints a simple study has been completed in which the number of each group is varied between 0 and 4, and the molecular constraints are applied. Considering the —CH_3, —CH_2—, >CH—, >C<, =CH_2 and =CH— groups this corresponds to a total of $5^6 = 15{,}625$ combinations. After applying the molecular constraints this results in a total of 320 feasible working fluids. Upon a manual inspection of these results it was observed that these 320 working-fluids included all the expected hydrocarbon families such as n-alkanes, methyl alkanes, 1-alkenes, 2-alkenes, alongside less typical, but chemically feasible combinations, thus validating the molecular feasibility constraints.

3.2. Validation of SAFT-γ Mie within an ORC model

Before applying the CAMD-ORC model to a WHR case study, it is necessary to validate that SAFT-γ Mie is suitable for determining the performance of ORC systems. Previously, a comparison between SAFT-γ Mie and the NIST REFPROP database was completed for the saturation properties of normal alkanes [58]. In our current paper this comparison is extended by solving the ORC model described in Section 2.3 using both SAFT-γ Mie and NIST REFPROP. The assumptions for this study are listed in Table 1, and using these assumptions the performance of an ORC system operating with different alkane working fluids has been evaluated over a range of reduced pressures. It should be noted that the heat source is assumed to be a pressurised liquid, with a defined specific heat capacity of 4.2 kJ/(kg K); such an assumption is valid since the thermodynamic optimum is independent of the heat-source heat-capacity rate (*i.e.*, $\dot{m}_{\mathrm{h}} c_{\mathrm{p,h}}$).

The results from this analysis are shown in Fig. 4. It is observed that the two approaches agree well, with very similar trends for both the power output and the thermal efficiency being obtained. Furthermore, both approaches yield the same maximum power point at the same reduced pressure. This therefore validates the SAFT-γ Mie equation of state for the performance prediction of ORC systems operating with alkane working fluids.

As an aside, the behaviour observed in Fig. 4 for the different working fluids can be explained since the molecular complexity (*i.e.*, the number of groups) is approximately proportional to the critical temperature. For example, *n*-pentane consists of two —CH_3 groups and three —CH_2— groups and has a critical temperature of 196.7 °C, whilst *n*-heptane has two additional —CH_2— groups and a critical temperature of 267.1 °C. Therefore, to obtain a similar evaporating temperature within the ORC, the *n*-heptane cycle must operate at a lower reduced pressure. Furthermore, a lower reduced pressure corresponds to a greater latent heat of vaporisation, which means a greater proportion of the heat absorbed by the working fluid from the heat source is used to evaporate the working fluid. Since evaporation occurs under isothermal conditions, this limits the temperature reduction in the heat source, leading to a higher average heat-source temperature and a higher thermal efficiency. However, this also leads to a lower working-fluid mass flow rate and lower power output. This trade-off between power output and thermal efficiency is a phenomenon that has been well discussed within the literature [60,61].

3.3. Validation of the optimisation model

In addition to comparing SAFT-γ Mie to NIST REFPROP, the developed model has also been compared to another CAMD-ORC optimisation study taken from the literature [54]. The authors of this previous study use an alternative SAFT equation of state, namely PC-SAFT [50,51], and for the assumptions listed in Table 1 they obtain a list of ten optimal working-fluids. From these ten working fluids, four alkane and three alkene working fluids were identified and using the approach outlined in Section 2, the ORC system was optimised. The results of our current optimisation in terms of the net power output and the condensation and evaporation pressures are compared to the PC-SAFT results in Fig. 5.

Overall, similar trends are observed for both the PC-SAFT and SAFT-γ Mie approaches in terms of the optimal evaporation and condensation pressure for each working fluid. However, when comparing PC-SAFT and SAFT-γ Mie in terms of the absolute power it is observed that SAFT-γ Mie always results in higher values; for propane and propene the percentage difference between SAFT-γ Mie and PC-SAFT is 4.4% and 7.0% respectively, whilst for the remaining fluids the difference is less than 2%. Having said this, in general the rankings of the working fluids from the two studies are similar, with relatively simple working fluids such as propane and propene being favoured over working fluids with increasing molecular complexity, although it also observed that these two fluids do have the highest operating pressures. Therefore, given that both SAFT-γ Mie and PC-SAFT both point towards a similar

Table 1
Model inputs for the two validation studies. The NIST study refers to the validation study completed using NIST REFPROP data, as discussed in Section 3.2. The PC-SAFT study refers to the validation study discussed in Section 3.3. Note that 'var.' denotes a variable parameter.

	T_{hi} (°C)	$c_{\mathrm{p,h}}$ J/(kg K)	$\dot{m}_{\mathrm{h}}$ (kg/s)	η_{p} (%)	η_{e} (%)	PP_{h} (°C)	T_1 (°C)	ΔT_{sh} (°C)
NIST	200	4200	1.0	70	80	10	30	10
PC-SAFT [54]	120	4200	66.0	90	80	10	var.	var.

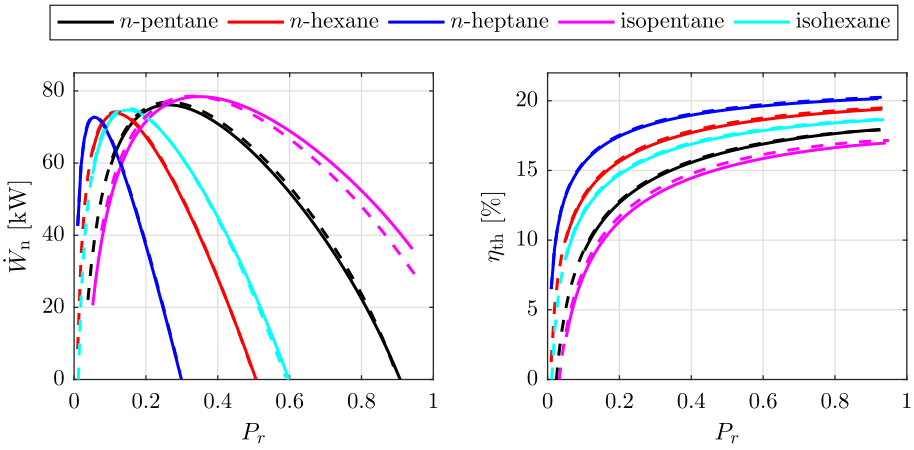

Fig. 4. Comparison between the net power $\dot{W}_{\mathrm{n}}$ and thermal efficiency η_{th}, as functions of reduced pressure, obtained from the ORC model when using SAFT-γ Mie (solid) and NIST REFPROP (dashed) for hydrocarbon working-fluids.

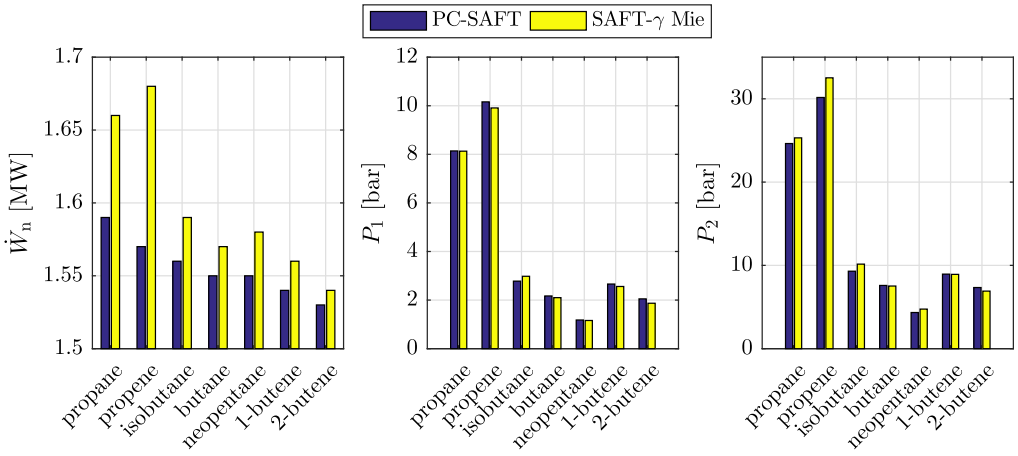

Fig. 5. Validation of the model against the optimisation study completed using PC-SAFT in Ref. [54].

optimum working fluid, and that the optimal ORC condensation and evaporation pressures are similar, this comparison further confirms the suitability of the SAFT-γ Mie equation of state, the ORC system model, and the optimisation framework.

4. Case study

4.1. Definition

Having confirmed that the CAMD-ORC model is suitable, it can now be applied to WHR applications. For this study three heat-source temperatures have been defined, namely $T_{hi} = 150$, 250 and 350 °C. These temperatures correspond to typical temperatures at which industrial waste heat is available, and temperatures at which an ORC system could be used. From a thermodynamic point of view, the optimal working fluid is independent of the heat-source heat capacity rate ($\dot{m}_h c_{p,h}$), and therefore the heat-source mass flow rate and specific heat capacity are set arbitrarily to 1 kg/s and 4.2 kJ/(kg K) respectively. The rest of the assumptions are listed in Table 2. The minimum allowable condensation pressure $P_{1,min}$ was set to 0.25 bar absolute.

Within this study, the CAMD-ORC MINLP optimisation model has been used to investigate and optimise several different families of hydrocarbon working fluids, namely *n*-alkanes, methyl alkanes, 1-alkenes and 2-alkenes. Each of these families consists of a specific set of molecular groups, but can include a variable number of —CH_2— groups. For example, an *n*-alkane is described by two —CH_3 groups and a number of —CH_2— groups, whilst a methyl alkane is described by three —CH_3 groups, one ≻CH— group and a number of —CH_2— groups. 1-alkenes and 2-alkenes are similarly described, although a 1-alkene contains a —CH_2═CH— double bond, whilst a 2-alkene contains a —CH═CH— double bond. The molecular structures of these four hydrocarbon families are summarised in Table 3.

Alongside the number of —CH_2— groups, the four ORC system variables can also be optimised to maximise the power output from the system. These optimisation variables are listed in Table 4, alongside their lower and upper bounds. During initial optimisation studies it was found that the opimiser failed when the degree of superheating ΔT_{sh} approached zero. To rectify this problem the lower bound for ΔT_{sh} was increased to 0.1 °C to avoid expansion directly from the saturated vapour state. However, the difference in performance between an optimal cycle with zero superheating, and the same cycle with $\Delta T_{sh} = 0.1$ °C will be negligible.

Table 3
Definition of the four hydrocarbon families considered within this study.

n-alkanes CH_3—$(CH_2)_n$—CH_3	methyl alkanes $(CH_3)_2$—CH—$(CH_2)_n$—CH_3
1-alkenes CH_2═CH—$(CH_2)_n$—CH_3	2-alkenes CH_3—CH═CH—$(CH_2)_n$—CH_3

Table 4
Optimisation variables defined for the WHR case study and their lower and upper bounds.

Variable	Lower bound	Upper bound	Unit
T_1	15	70	°C
P_r	0.001	0.85	–
ΔT_{sh}	0.1	200	°C
PP_h	10	200	°C
—$(CH_2)_n$—	0	20	–

4.2. Parametric NLP study

Before completing the full CAMD-ORC MINLP optimisation study, a parametric NLP optimisation study was completed whereby for each hydrocarbon family the number of —CH_2— groups was varied parametrically and an NLP optimisation considering only the ORC system variables was completed. After obtaining the optimal system design for each predefined working fluid, the number of —CH_2— groups was then introduced as a continuous variable and another NLP optimisation was completed. The result from this optimisation should provide the global maximum of

Table 2
Defined model inputs for the three WHR case studies conducted with heat source temperatures of 150, 250 and 350 °C respectively.

$c_{p,h}$ J/(kg K)	$\dot{m}_h$ (kg/s)	T_{ci} (°C)	$c_{p,c}$ J/(kg K)	$\dot{m}_c$ (kg/s)	η_p (%)	η_e (%)	$PP_{c,min}$ (°C)	$P_{1,min}$ (bar)
4200	1.0	15	4200	5.0	70	80	5	0.25

the objective function for that hydrocarbon family. Finally, a few additional NLP optimisation studies were completed setting the number of —CH_2— groups to a non-integer value that is close to the theoretical optimum. This was done to ensure the NLP optimisation successfully finds the global optimum, and to allow the behaviour of the system as the number of —CH_2— groups changes to be investigated. The results from this study for the four different hydrocarbon families listed in Table 3, at the three different heat-source temperatures, are displayed in Fig. 6.

Firstly, in all instances the NLP optimisation that incorporated the number of —CH_2— groups as a continuous variable always resulted in the highest net power output from the system, thus confirming that when optimising the five variables listed in Table 4, the NLP optimisation always finds the global optimum. For the three-defined heat sources this corresponds to maximum net output powers of 36.4, 138.0 and 227.0 kW respectively. For the 150 °C heat source, this optimum was found for a 1-alkene, whilst for the other two heat-source temperatures this optimum was found for a 2-alkene.

Secondly, it is observed that around the optimum number of —CH_2— groups there is often a steep reduction in the power output as the number of —CH_2— groups either increases or decreases from this optimal point, and this leads to feasible systems (*i.e.*, an integer number of —CH_2— groups) with lower power outputs. For example, considering the 1-alkene family for the 150 °C heat source, the theoretical maximum power is 36.4 kW at —$(CH_2)_n$— = 0.3. However, reducing this to —$(CH_2)_n$— = 0.0 or increasing to —$(CH_2)_n$— = 1 reduces the power output by 4.5% and 8.6% respectively. To understand this behaviour in more detail the results for this hydrocarbon family for this heat-source temperature have been presented in Fig. 7. Here the optimal ORC system variables, and the resulting net power output are presented against the number of —CH_2— groups. The condensation temperature and evaporator pinch point have not been included since the condensation temperature was found to vary only by a few degrees, whilst the optimal pinch point always sat at the lower bound of 10 °C.

From Fig. 7, it is observed that the global optimum corresponds to the number of —CH_2— groups that maximises the net power output from the system, whilst having the maximum possible reduced pressure ($P_r = 0.85$) and the minimum superheat ($\Delta T_{sh} = 0.1$ °C). As the number of —CH_2— groups reduces, the critical temperature of the fluid will reduce and therefore the maximum evaporation temperature will also reduce. Therefore, to effectively utilise the heat available it is necessary start superheating the working fluid. Conversely, as the number of —CH_2— groups

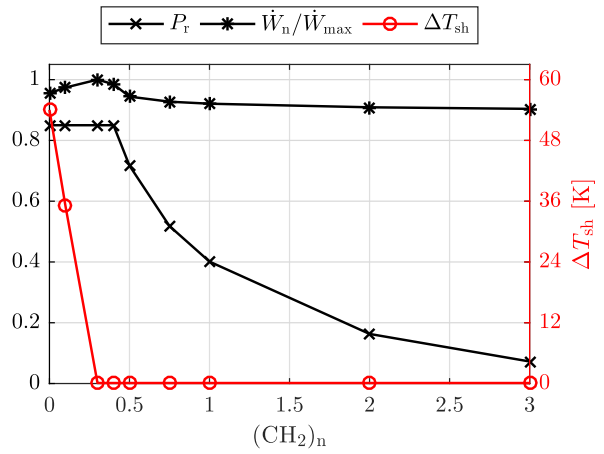

Fig. 7. The variation in the optimal reduced pressure P_r, the normalised power output $\dot{W}_n/\dot{W}_{max}$ and the optimal amount of superheating ΔT_{sh} as a function of the number of —CH_2— groups for the 1-alkene family and a heat-source temperature of $T_{hi} = 150$ °C.

increases, the critical temperature of the fluid increases, so the reduced pressure will reduce to maintain a similar evaporation temperature and therefore heat-source profile. In other words, during the NLP optimisation in which the integer optimisation variables are relaxed and can take any continuous value, the optimisation converges on an optimum theoretical working-fluid that operates at the maximum bound for the reduced pressure, and minimum bounds for the amount of superheating and the evaporator pinch point.

The results in Fig. 6 have been replotted in terms of the number of carbon atoms contained within the working-fluid, and these results are shown in Fig. 8. From this figure, it is clear that for each heat-source temperature there appears to be an optimum number of carbon atoms that the working fluid should contain if one wants to maximise the net power output from the system. It is also observed that as the heat-source temperature increases, increasingly complex working fluids should be favoured. For this study, it appears that the number of carbon atoms should be around 3, 5 and 6–7 for heat-source temperatures of 150, 250 and 350 °C respectively. This information can immediately be used to identify likely working fluids for these heat-source temperatures.

Finally to conclude this section it is necessary to discuss the effect of the working fluid on the ORC condensation temperature

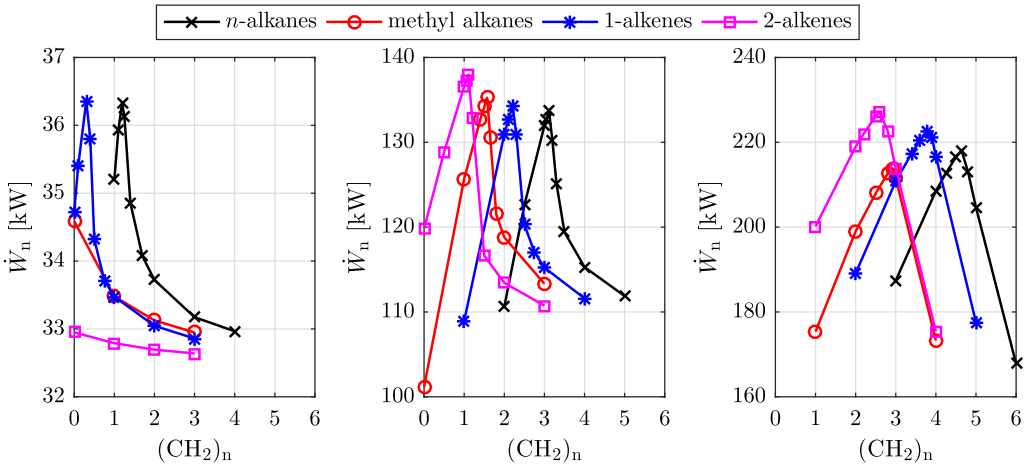

Fig. 6. The effect of the number of —CH_2— groups on the net power output from the ORC system for the four hydrocarbon families at three different heat-source temperatures; from left to right: $T_{hi} = 150,\ 250$ and 350 °C.

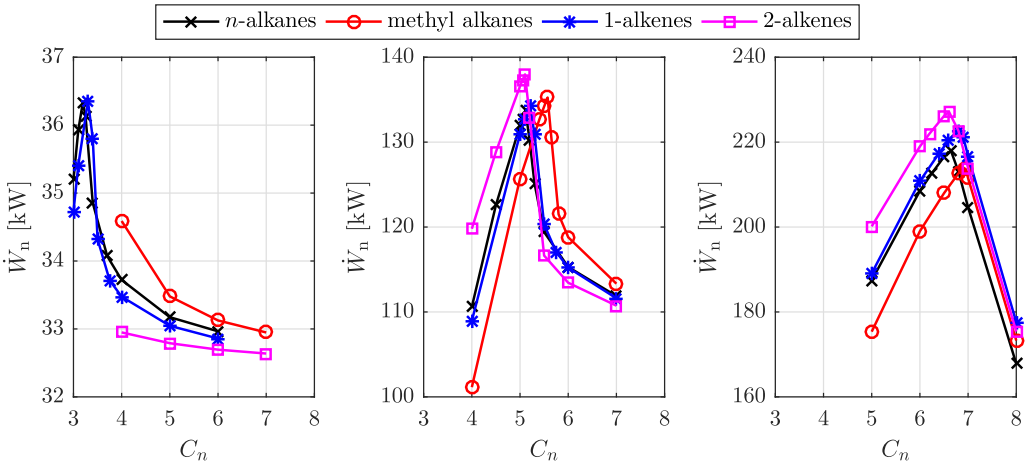

Fig. 8. The results from Fig. 6 represented in terms of the number of carbon atoms C_n, rather than the number of —CH_2— groups; from left to right: $T_{hi} = 150,\ 250$ and 350 °C.

and pressure. Although not shown in Fig. 7, the optimal condensation temperature for the 150 and 250 °C heat sources is found to be the minimum condensation temperature that can be obtained without violating the condenser pinch constraint. However, when considering the 350 °C heat source, the condensation temperature is no longer constrained by the condenser pinch point, but instead is constrained by the minimum allowable condensation pressure, defined here as 0.25 bar absolute. This is because as the molecular complexity of the working-fluid increases, the saturation temperature at this defined pressure also increases. For example, for the 150 °C heat source the optimal condensation temperatures range between 31.6 and 35.4 °C, with condensation pressures between 2.7 and 9.7 bar absolute. However, for the 350 °C heat source all condensation pressures are 0.25 bar absolute, whilst the condensation temperatures have increased to values between 46.6 and 47.3 °C. The minimum allowable condensation pressure was defined as 0.25 bar absolute as this value was considered to be a reasonable trade-off between the additional performance benefit that sub-atmospheric condensation offers, and the additional complexity of having to design a sub-atmospheric condenser.

To investigate the effect of the condensation pressure constraint on the cycle the NLP optimisations for the 350 °C heat source were repeated, this time setting $P_{1,min} = 0$ bar absolute. The results are shown in Fig. 9.

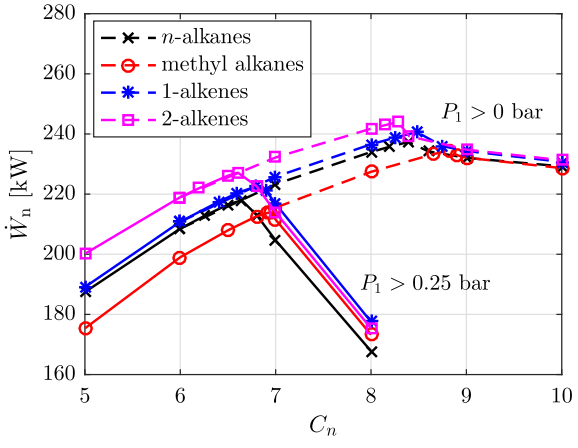

Fig. 9. The effect of the condensation pressure constraint on the net power output from the cycle for the 350 °C heat source. The solid lines correspond to the 0.25 bar absolute constraint, whilst the dashed lines correspond to the unconstrained optimisation cases.

From Fig. 9 it is clear that the condensation pressure constraint limits the maximum power output that can be generated from the system. For less complex molecules, with $C_n = 6$, both optimisations result in the same optimal cycle since the condensation temperature is not constrained by the condensation pressure. However, as molecular complexity increases, the 0.25 bar constraint causes a reduction in the power output, and also results in an optimal working fluid that contains less carbon atoms than the optimum obtained from the unconstrained optimisation. For the results shown in Fig. 9, the condensation pressure constraint reduces the maximum theoretical power output by 6% when compared to the unconstrained optimisation, and ultimately results in the selection of a molecule composed of 6 or 7 carbon atoms, rather than 8 or 9. Therefore, this analysis clearly demonstrates the improved thermodynamic performance that can be achieved for high-temperature heat sources by using more complex molecules, but highlights the complexity of having to operate these fluids under a vacuum in order to realise their potential.

4.3. MINLP study

The final stage of this study was to set the number of —CH_2— groups to an integer decision variable and to run the full CAMD-ORC MINLP optimisation problem. Clearly, the optimal integer number of —CH_2— groups for each hydrocarbon family is already known from either Figs. 6 or 8. However, the purpose of now completing the MINLP optimisation is to confirm the suitability of the MINLP solver for CAMD-ORC problems. Furthermore, for each hydrocarbon family and heat-source temperature the MINLP optimisation was completed for multiple starting points to ensure that the global optimum was found. These starting points were defined as the optimal points that resulted from the initial parametric NLP optimisation study. For example, for the *n*-alkane family and 150 °C heat source, an optimal ORC system was obtained for *n*-propane, *n*-butane, *n*-pentane and *n*-hexane, and for this case these results were used as the MINLP starting points.

For each hydrocarbon family and heat-source temperature it was found that all starting points converged to the same optimal number of —CH_2— groups and the same values for the ORC system variables. Furthermore, the optimal system that results from the MINLP optimisation also matched the optimal systems identified in the previous parametric NLP study, therefore confirming the suitability of the MINLP solver. The resulting net power output for each case is summarised in Fig. 10. For the 150, 250 and 350 °C heat-source temperatures optimal net power outputs of 35.2, 136.7 and 219.0 kW are obtained respectively. For the

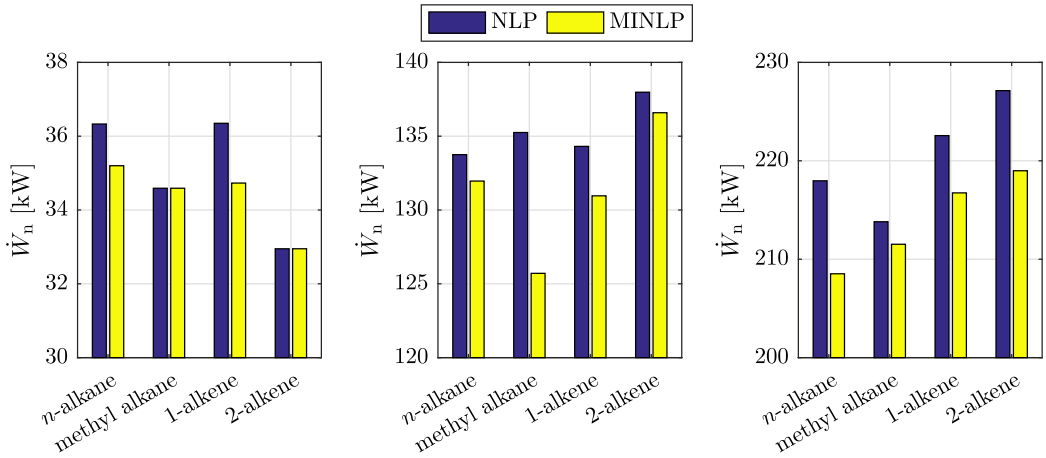

Fig. 10. The maximum net power output obtained from each heat source with each hydrocarbon family. The NLP results refer to the theoretical maximum obtained from the NLP study, whilst the MINLP results refer to the maximum that can be achieved using a feasible working-fluid; from left to right: $T_{hi} = 150,\ 250$ and 350 °C.

150 °C heat source this is obtained for propane (CH_2—CH_3—CH_2) which is part of the *n*-alkane family, whilst for the 250 and 350 °C heat sources both fluids are part of the 2-alkene family, with 2-pentene (CH_3—CH=CH—CH_2—CH_3) and 2-hexene (CH_3—CH=CH—$(CH_2)_2$—CH_3) being the optimal working-fluids respectively.

From Fig. 10, it is also observed that the percentage reduction in the net power output from the MINLP optimisation studies compared to the theoretical maximums range between 0% and 7.1%. The 0% corresponds to the methyl alkane and 2-alkene families for the 150 °C heat source, in which both the NLP and MINLP both converged on solutions with zero —CH_2— groups. The largest percentage difference corresponds to the methyl alkane family for the 250 °C heat source, and in this case the NLP converged on a solution with 1.57 —CH_2— groups. Since this is not particularly close to either 1 or 2 —CH_2— groups, a significant reduction in power is observed when moving to the MINLP result.

Overall, this study suggests that propane is an optimal working fluid for temperatures below 150 °C, and this agrees well with the study performed using PC-SAFT in Ref. [54]. Furthermore, these results suggest that working fluids that contain a CH=CH double bond (*i.e.*, 2-alkenes) perform well for heat-source temperatures between 250 and 350 °C. More generally, the results from the present study have confirmed the suitability of the CAMD-ORC model for the integrated working fluid and thermodynamic optimisation of ORC systems. Instead of running multiple optimisations for a range of different working fluids, one MINLP optimisation can be completed for each hydrocarbon family to determine the optimal working fluid and thermodynamic parameters. This demonstrates the potential of the CAMD-ORC formulation to drive the search for the next generation of ORC systems. In the future, further complexity will be added into the optimisation process to enable the consideration of more complex molecules, in addition to a wider range of molecular groups.

5. Beyond thermodynamic modelling: Sizing and cost correlations

The uptake of organic Rankine cycle systems (and low-grade waste-heat recovery technologies in general) has been hindered by their unfavourable economics underscored by their high specific investment costs and break-even times. Thus, it is crucial to explore avenues through which the costs of the ORC system components can be reduced. This is especially true for the heat exchangers (preheaters, evaporators and condensers) and the expander, which collectively, can contribute over 95% of the total component costs in medium- to low-power ORC systems [62]. Therefore, to use the CAMD-ORC model to develop ORC systems that are cost-effective whilst having good thermal performance it is necessary to extend the CAMD-ORC model beyond the thermodynamic analysis previously presented. By introducing component sizing models for the key system components, it will, in the future, be possible to introduce component cost correlations and to optimise the working-fluid and ORC system on the basis of thermoeconomic performance indicators such as the payback period, net-present value or the levelised cost of electricity. The following section investigates group-contribution methods for determining the transport properties of hydrocarbon working-fluids, in addition to considering expander and pump performance with reference to the case study presented in Section 4.

5.1. Transport property prediction for heat exchanger modelling

A key step in the sizing of heat exchangers is the estimation of the heat transfer coefficients for the different fluid phases. This process relies heavily on various experimentally-derived correlations which are functions of well-established dimensionless numbers *e.g.*, the Nusselt and Prandtl numbers. These numbers are ratios of combinations of thermodynamic and transport properties, including their thermal conductivity and dynamic viscosity. While the SAFT-based equations of state [55,57] can reliably provide the required thermodynamic properties, they do not allow for the calculation of fluid transport properties.

Thus, the required transport properties, specifically the dynamic viscosity, thermal conductivity and surface tension, have to be predicted by other means. While there are numerous property-estimation methods, for example those detailed in Ref. [63], the methods to be used for this work need to fulfil certain criteria. Firstly, the methods should be applicable to a large number of fluids and homologous series. Also, they should be fairly straight-forward to implement; methods that require solving for roots of equations and/or solving differential equations may not be appropriate here. In particular, transport-property prediction methods that incorporate molecular group-contribution approaches are sought, in line with the motivation and modelling objective and framework in this work. Methods that are found suitable for the hydrocarbon working fluids considered within this study (*n*-alkanes, methyl alkanes, 1-alkenes and 2-alkenes) are summarised below.

5.1.1. Necessary thermodynamic properties

The transport-property prediction methods that will be highlighted below are generally empirical correlations, that incorporate elements of group-contribution approaches, and in some instances rely on thermodynamic quantities such as the normal boiling temperature, molecular weight and molar densities. Also, these methods generally consider the specific fluid phases (liquid or vapour phase respectively) and as such an equation of state will be required for the prediction of these quantities. Correlations for estimating the vapour-phase thermal conductivity require the constant-volume specific heat capacity (c_v) and vapour density which are obtainable from the SAFT-γ Mie equation of state as functions of temperature and pressure (and composition, for mixtures).

Another thermodynamic quantity that is required is the normal boiling temperature, T_b, or its reduced form, $T_{b,r} = T_b/T_{cr}$. While experimental values of T_b are available, they can also be obtained easily from SAFT-γ Mie to a high degree of accuracy. This high degree of accuracy is made possible because experimental P–T saturation data are used for the estimation of model parameters for the molecular groups. Similarly, experimental values of single-phase densities can be accurately predicted by SAFT-γ Mie because these values were used in the estimation of the group-contribution model parameters.

Other required thermodynamic quantities include the critical temperature T_{cr}, critical pressure P_{cr} and critical (molar) volume V_{cr}, and the acentric factor. Analogous to the estimation of P_{cr}, described in Section 2.3, T_{cr} (in K) and V_{cr} (in cm^3/mol) are estimated from the Joback and Reid correlations [29]:

$$T_{cr} = T_b\left[0.584 + 0.965\sum_i T_{cr,i} - \left(\sum_i T_{cr,i}\right)^2\right]^{-1}, \tag{13}$$

and:

$$V_{cr} = 17.5 + \sum_i V_{cr,i}, \tag{14}$$

where T_b is the normal boiling temperature obtained from SAFT-γ Mie, and $T_{cr,i}$ and $V_{cr,i}$ are the individual critical temperature and critical volume contributions from each molecular group i, as given in Ref. [29].

While other methods exist for estimating the critical properties, they are either less accurate or do not have the same type of group classifications required in this work. An example is the method of Constantinou and Gani [64] which uses olefinic groups of the CH_2–=CH—, —CH=CH—, CH_2=C<, —CH=C< and >C=C< types, as opposed to the =CH_2, =CH—, =C< and =C= groups considered within this current work. In addition, this method shows large errors in estimating the critical properties of compounds with a low number of carbon atoms such as ethane and propane.

The only other required quantity is the acentric factor (ω), which is estimated by solving the Pitzer vapour pressure expansion:

$$\ln P_{vp,r} = f^{(0)} + \omega f^{(1)} + \omega^2 f^{(2)}, \tag{15}$$

for ω, at the atmospheric pressure and normal boiling temperature, and ignoring the quadratic term which has been shown to have no effect on the result [63]. This results in the expression:

$$\omega = -\frac{\ln(P_{cr}/1.01325) + f^{(0)}}{f^{(1)}}, \tag{16}$$

where $f^{(0)}$ and $f^{(1)}$, at the normal boiling temperature, are given by Ambrose and Walton [65] as:

$$f^{(0)} = \frac{-5.97616\tau + 1.29874\tau^{1.5} - 0.60394\tau^{2.5} - 1.06841\tau^5}{T_{b,r}};$$
$$f^{(1)} = \frac{-5.03365\tau + 1.11505\tau^{1.5} - 5.41217\tau^{2.5} - 7.46628\tau^5}{T_{b,r}}; \tag{17}$$

with $\tau = 1 - T_{b,r}$ and $T_{b,r} = T_b/T_{cr}$.

Using the estimated critical properties from the Joback and Reid correlations (Eqs. (7) and (13)), acentric factor predictions from Eq. (16) were compared with those from the original Pitzer et al. definition ($\omega = -\log_{10}[\lim_{(T/T_{cr})=0.7} P_{vp}/P_{cr}] - 1.0$ [66], also made using the predicted critical properties) for the 17 hydrocarbon fluids in this section. Both sets of predictions were quite close to the true values of ω (*i.e.*, those obtainable from the Pitzer et al. definition, but using experimental values of the critical properties), with the percentage deviation less than 5.0% for most of the fluids. However, using Eq. (16) generally resulted in predicted ω values with lower percentage deviations than those made using the Pitzer et al. definition with estimated critical properties.

With these thermodynamic properties provided, the required transport properties can then be estimated.

5.1.2. Dynamic viscosity

5.1.2.1. Liquid dynamic viscosity. The dynamic viscosities of liquid *n*-alkanes can be accurately predicted by the Joback and Reid group contribution method [29] which uses a two-parameter equation to describe the temperature dependency of the dynamic viscosity:

$$\eta_L = M\ \exp\left[\left(\sum_i \eta_{a,i} - 597.82\right)/T + \sum_i \eta_{b,i} - 11.202\right], \tag{18}$$

where η_L is the liquid viscosity in units of Pa s and M is the molecular weight of the molecule. The contributions from each group ($\eta_{a,i}$ and $\eta_{b,i}$) considered in this paper can be found in Joback and Reid [29]. This method however gives predictions with large errors for the liquid viscosities of branched alkanes. For these molecules, an alternative method, the Sastri-Rao method [67] is employed. The pure-liquid viscosity in units of mPa s is calculated with the equation:

$$\eta_L = \sum_i \eta_{B,i} \times P_{vp}^{-\left[0.2+\sum_i N_i\right]}. \tag{19}$$

The values for the group contributions to determine the summations above are given in Ref. [67]. The contributions are generally cumulative, except for the case of $\sum_i N_i$ where the contributions from each functional group are taken only once (*e.g.*, in 2-methylpentane, the contributions from the —CH_3 groups are taken once, not three times while those from the —CH_2 groups are also taken once instead of twice). The vapour pressure (P_{vp}, in atmospheres) is calculated as a function of the normal boiling point, T_b:

$$\ln P_{vp} = (4.5398 + 1.0309\ln T_b) \times \left(1 - \frac{(3 - 2T/T_b)^{0.19}}{T/T_b} - 0.38(3 - 2T/T_b)^{0.19}\ln(T/T_b)\right). \tag{20}$$

The switch between the Joback and Reid method and the Sastri-Rao method for alkanes can be easily implemented by employing the Sastri-Rao method when the number of —CH_3 groups is three or greater and using the Joback and Reid method otherwise.

5.1.2.2. Vapour dynamic viscosity. For the vapour phases, the dynamic viscosities (in units of microPoise) are calculated using

the corresponding states relation suggested by Reichenberg [68,69]:

$$\eta_V = \frac{M^{1/2}T}{\sum_i n_i C_i [1 + (4/T_{cr})][1 + 0.36T_r(T_r - 1)]^{1/6}} \times \frac{T_r(1 + 270\mu_r^4)}{T_r + 270\mu_r^4}, \quad (21)$$

where n_i represents the number of groups of the ith type and C_i is the group contribution available from Refs. [68,69]. μ_r is the reduced dipole moment and $T_r = T/T_{cr}$ is the reduced temperature. For high pressure fluids, a correction factor is provided by Reichenberg [70,71]:

$$\frac{\eta_V}{\eta_{V,0}} = 1 + Q\frac{AP_r^{3/2}}{BP_r + (1 + CP_r^D)^{-1}}. \quad (22)$$

The constants A, B, C and D are functions of T_r as shown below and $\eta_{V,0}$ is the vapour viscosity at the same temperature and low pressure from Eq. (21). $Q = 1 - 5.655\mu_r$; $Q = 1.0$ for non-polar molecules.

$$\begin{aligned} A &= \tfrac{1.9824\times10^{-3}}{T_r}\exp 5.2683T_r^{-0.5767};\\ B &= A(1.6552T_r - 1.2760);\\ C &= \tfrac{0.1319}{T_r}\exp 3.7035T_r^{-79.8678};\\ D &= \tfrac{2.9496}{T_r}\exp 2.9190T_r^{-16.6169}. \end{aligned} \quad (23)$$

These equations should be used with caution as C and D approach infinity at low values of T_r.

Another applicable method for the estimation of vapour viscosity is that of Chung et al. [72,73], including their modification for high-pressure systems. This method however requires special correction factors that are compound specific and, as such, does not fit well with the group-contribution basis of this work.

The predicted dynamic viscosities from the aforementioned group-contribution theories (for both the liquid and vapour phases) are compared with the available psuedo-experimental values from the NIST REFPROP database at temperatures between 0 °C and 400 °C. The comparisons for the *n*-alkanes, the methyl alkanes and the alkenes are presented in Fig. 11; only the few methyl alkanes and alkenes available in REFPROP have been presented here. The *n*-alkanes and methyl alkanes are in the subcooled liquid state at lower temperatures and in the supreheated vapour state at higher temperatures (>200 °C) while the alkenes are in the vapour state at all temperatures. The predictions from the group-contribution methods are seen to be in good agreement with the experimental data from REFPROP. The vapour-phase viscosities are predicted by the Reichenberg relation in Eq. (21) while the liquid-phase viscosities are predicted with the Joback and Reid method in Eq. (18), with the exception of those of the methyl alkanes which are predicted with the Sastri-Rao method in Eq. (19).

5.1.3. Thermal conductivity

5.1.3.1. Liquid thermal conductivity. Most estimation techniques for the thermal conductivity of liquids are empirical in nature. Two methods, the Latini et al. method [74–76] and the Sastri method [77] often appear rather accurate [63]. Latini and coworkers suggested a correlation requiring specific parameters for various classes of organic compound and specific parameters for various compounds [76]. This makes the correlation inconvenient for a group-contribution calculation; the Sastri method, however, allows for group contributions to the thermal conductivity:

$$\lambda_L = \sum_i \lambda_{b,i} \times a^m, \quad (24)$$

where

$$m = 1 - \left(\frac{1 - T_r}{1 - T_{b,r}}\right)^n, \quad (25)$$

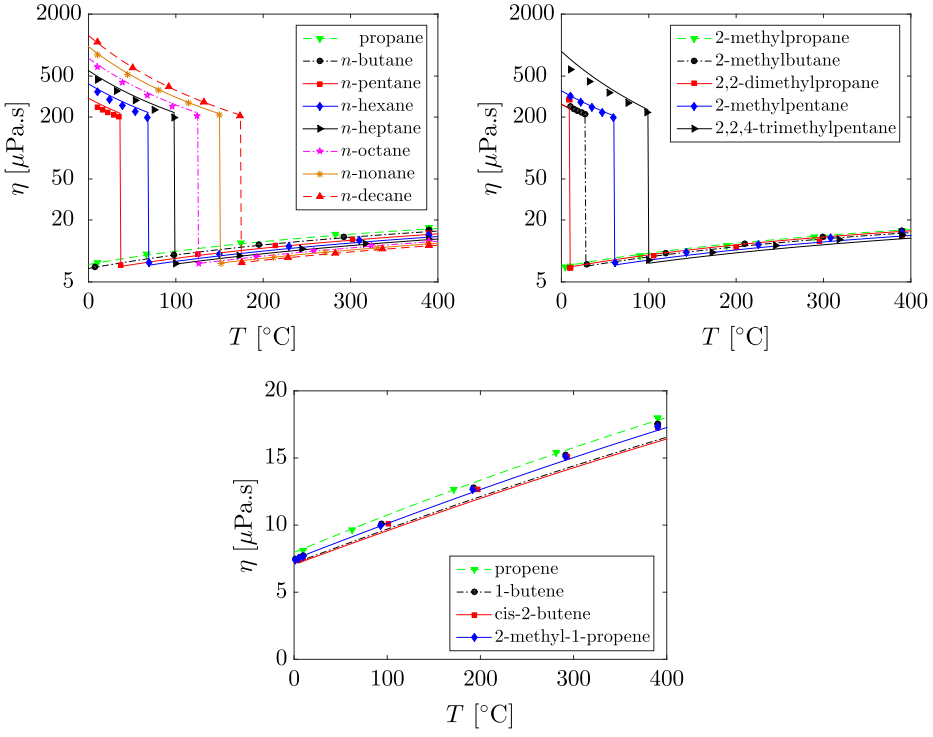

Fig. 11. Low-pressure dynamic viscosity of *n*-alkanes, methyl alkanes and alkenes, in the liquid and vapour phases as functions of temperature. Comparison of predicted viscosities from the group-contribution theories (continuous curves) with experimental data from the NIST REFPROP database (symbols).

with $a = 0.856$ and $n = 1.23$ for alcohols and phenols, or $a = 0.16$ and $n = 0.2$ for other compounds, and $\lambda_{b,i}$ (in units of W/(m K)) is the group contribution to the thermal conductivity at the normal boiling point; these values are available in Ref. [77].

For hydrocarbon compounds when the number of carbon atoms (C_n) is less than 5, a correction of $0.0150(5 - C_n)$ W/(m K) is added to $\sum_i \lambda_{b,i}$ in Eq. (24).

5.1.3.2. Vapour thermal conductivity. Notable methods for estimating the vapour-phase thermal conductivities include the Eucken equation, the modified Eucken correlation [78], the Stiel and Thodos equation [79], and the Chung et al. method [72,73]. These methods usually employ a relation of the dimensionless group, Eucken factor ($\lambda M'/\eta c_v$) as a function of thermodynamic variables such as c_v, T_r and ω. The Eucken factor is close to 2.5 for monoatomic gases but generally expected to be much less for polyatomic gases. The Eucken equation underestimates the conductivity while its modified form overestimates the conductivity and the Stiel and Thodos equation yields values between the two Eucken forms [63]; all three forms predict that the Eucken factor should decrease with temperature whereas the factor appears to increase slightly with temperature.

The Chung et al. method [72,73] tends to predict the correct trend of the factor with temperature and yields values close to those reported experimentally [63]. The thermal conductivity relation is given as:

$$\frac{\lambda_V M'}{\eta_V c_v} = \frac{3.75\Psi}{c_v/R}. \tag{26}$$

The variables in this equation are expressed in SI units (M' is the molar mass in kg/mol and $R = 8.314$ J/(mol K)), and c_v (in J/(mol K)) is obtainable from an equation of state such as the SAFT-γ Mie. The factor Ψ is calculated as:

$$\Psi = 1 + \alpha\{[0.215 + 0.28288\alpha - 1.061\beta + 0.26665Z] / [0.6366 + \beta Z + 1.061\alpha\beta]\}, \tag{27}$$

where

$$\alpha = c_v/R - 3/2; \quad \beta = 0.7862 - 0.7109\omega + 1.3168\omega^2; \quad Z = 2.0 + 10.5T_r^2. \tag{28}$$

Eq. (26) is modified to treat materials at high pressures, resulting in the following expression for the thermal conductivity:

$$\lambda_V = \frac{31.2\eta_V \Psi}{M'}(G_2^{-1} + B_6 y) + qB_7 y^2 T_r^{1/2} G_2. \tag{29}$$

In the above equation, $y = V_{cr}/(6V)$ and $q = 3.586\times 10^{-3}(T_{cr}/M')^{1/2}/V_{cr}^{2/3}$, where V_{cr} is the critical (molar) volume in cm^3/mol. The molar volume V_m, in cm^3/mol, is also obtainable from the SAFT-γ Mie equation of state (from the vapour density). The constants G_2, B_6 and B_7 are provided in Ref. [73]. At low pressures, V_m becomes large and y approaches zero and G_2 approaches unity, and the above equation will reduce to Eq. (26) for low pressure vapours.

In a similar manner to the dynamic viscosity, the predicted thermal conductivities are compared with the available experimental values from the NIST REFPROP database and presented in Fig. 12. The thermal conductivity predictions from the group-contribution methods are also seen to be in good agreement with the experimental data from REFPROP. The vapour-phase thermal conductivities are predicted with the Chung et al. method in Eq. (26) while the liquid-phase thermal conductivities are predicted with the Sastri method in Eq. (24).

5.1.4. Liquid surface tension

Several empirical corresponding states correlations are available for the estimation of the surface tension of the various chemical families of fluids. Sastri and Rao [80] present a modification of the corresponding-states methods to deal with polar liquids:

$$\sigma = KP_{cr}^x T_b^y T_{cr}^z \left[\frac{1 - T_r}{1 - T_{b,r}}\right]^m, \tag{30}$$

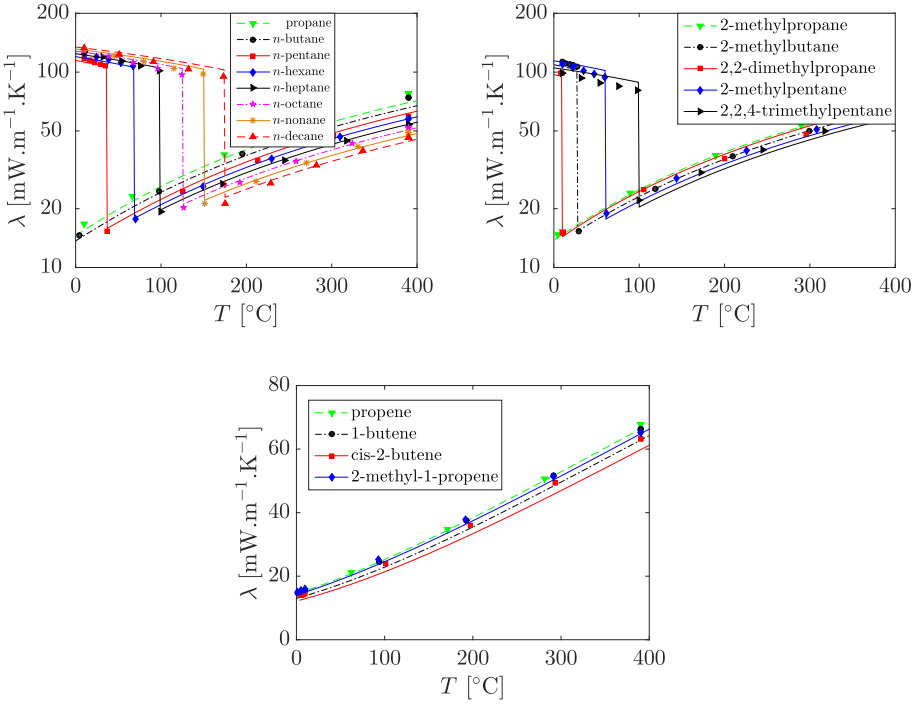

Fig. 12. Low-pressure thermal conductivity of *n*-alkanes, methyl alkanes and alkenes, in the liquid and vapour phases as functions of temperature. Comparison of predicted conductivities from the group-contribution theories (continuous curves) with experimental data from the NIST REFPROP database (symbols).

where σ is the surface tension in mN m^{-1}, and the pressure and temperature terms are in units of Kelvin and bar respectively. The values of the constants for alcohols and acids are available in Ref. [80] while for all other families of compounds, $K = 0.158$, $x = 0.50$, $y = -1.5$, $z = 1.85$ and $m = 11/9$.

Using the correlation presented in Eq. (30) the saturated-liquid surface tension of hydrocarbon working fluids can be predicted, and these predictions are compared with the available experimental data from REFPROP. The results are presented in Fig. 13. It should be noted that there are no experimental surface tension data for 2,2-dimethylpropane and cis-2-butene from REFPROP. For the compounds with available experimental data, the predictions from Eq. (30) are generally in good agreement with the experimental values, up to the critical point.

5.2. Expander and pump modelling

The expander is arguably the most critical component within the ORC system. Expander selection is typically governed by the size of the system, which is dependent on the amount of heat available, and also on the pressure or volume ratio across the expander, which in turn is a function of the heat-source temperature.

The optimal cycles determined in the optimisation study in Section 4 range between approximately 30 kW for the 150 °C heat source, and 230 kW for the 350 °C heat source. For the 30 kW system positive-displacement expanders would typically be favoured due to their simplicity, low rotational speeds and low costs. However, as the system size increases, more sophisticated turboexpanders would be selected due to their higher isentropic efficiencies.

In relation to the pressure and volume ratios, the results from the optimisation completed in Section 4 have been plotted in terms of these parameters in Figs. 14 and 15. Unsurprisingly it is observed that as the heat-source temperature increases both the volume ratio and pressure ratio increase. More interestingly though, it is also observed both ratios generally increase as the complexity of the molecule increases. Predominantly this can be attributed to the reducing condensation pressure as the number of carbon atoms increases, thus leading to low pressures and high specific volumes at the expander outlet. Furthermore, it is also observed that both the volume ratio and pressure ratio experience a peak at a particular number of carbon atoms, and this peak also corresponds to the maximum power point for that hydrocarbon family. It therefore follows that the optimal cycle obtained from the thermodynamic optimisation is the one that maximises the ORC pressure ratio, and therefore expander volume ratio.

Since high expander volume ratios have a significant impact on expander design, either through large built-in volume ratios for positive-displacement expanders, or large changes in flow area in a turboexpander, the effect of the working fluid on the expander performance cannot be overlooked. For the 150 °C heat source, the volume ratios observed could be achieved using a positive-displacement expander such as a screw expander. However, the higher volume ratios observed for the other two heat-source temperatures would require alternative expanders such as a reciprocating-piston expander or a radial turbine. Reciprocating-piston expanders are still at an early stage of development for ORC applications, but radial turbines are already used within commercial ORC units [81]. Therefore a radial turbine design model has been incorporated into the CAMD-ORC model, which is used to determine the rotor inlet blade velocity u and the rotor inlet Mach number Ma. The key details of the radial turbine model are presented in Appendix A, and the resulting Mach numbers obtained from the model are presented in Fig. 16.

Firstly, it is worth noting that the rotor inlet blade velocity ranged between 233 and 261 m/s (150 °C), 320 and 367 m/s (250 °C) and 381 and 440 m/s (350 °C) respectively, which all lie within the feasible range of tip speeds for radial turbines. In terms of the rotor inlet Mach number, an increase is observed as the heat-source temperature increases. It is also observed that the Mach number appears to increase as the molecular complexity of the working fluid increases; however, this is more likely due to the

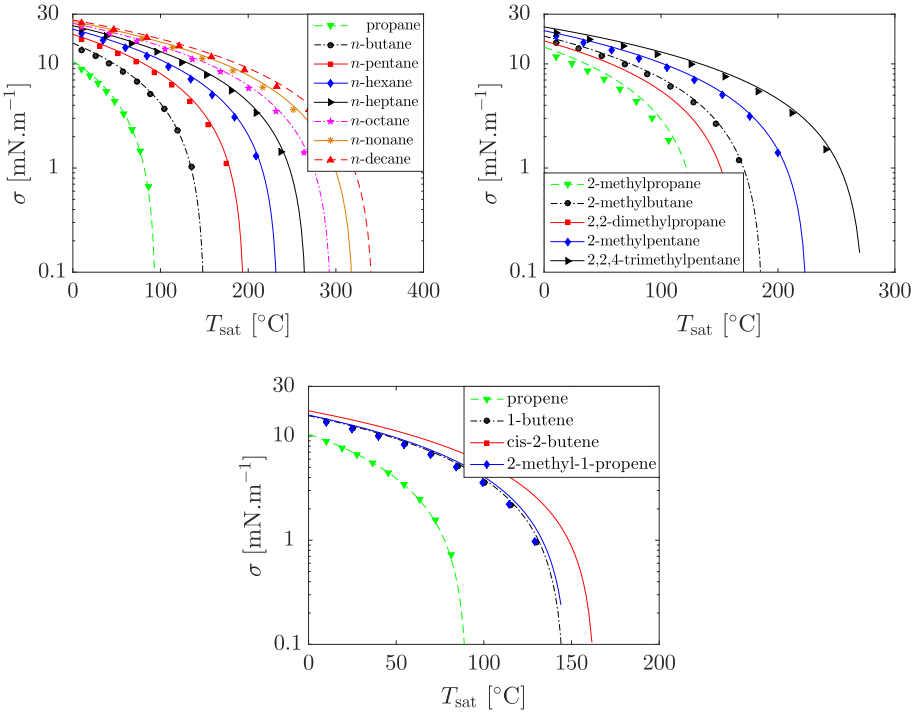

Fig. 13. Saturated-liquid surface tension of *n*-alkanes, methyl alkanes and alkenes. Comparison of predicted surface tension from the group-contribution theories (continuous curves) with experimental data from the NIST REFPROP database (symbols).

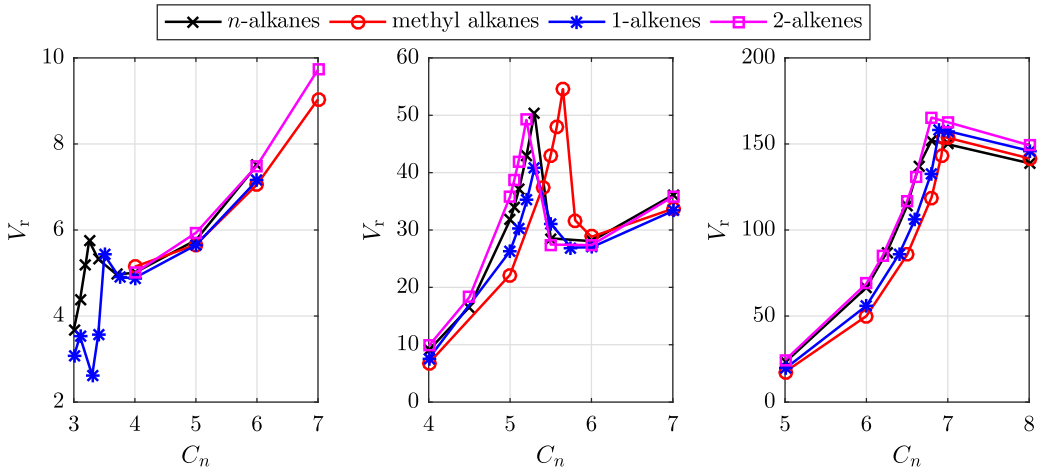

Fig. 14. The expander volume ratio as a function of the number of carbon atoms C_n obtained for each heat source temperature and hydrocarbon family; from left to right: $T_{hi} = 150,\ 250$ and 350 °C.

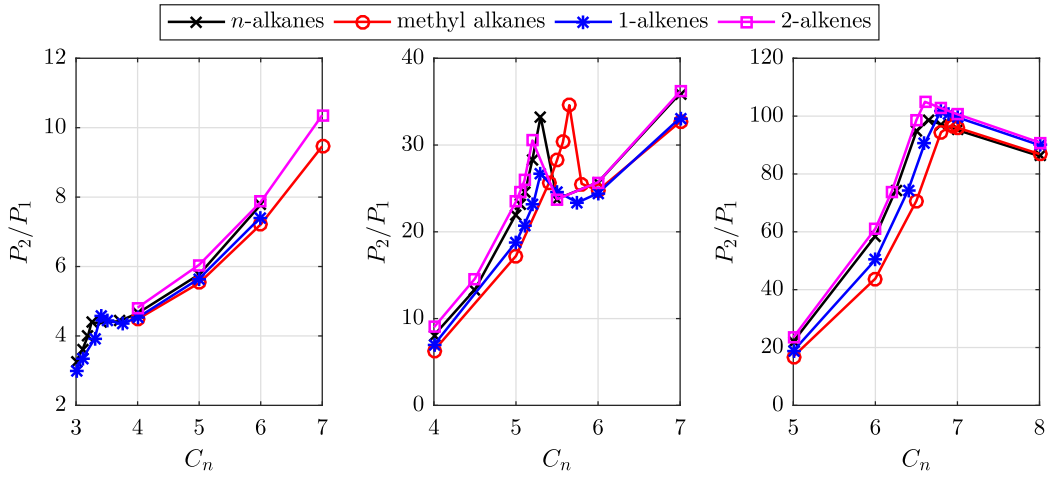

Fig. 15. The expander pressure ratio as a function of the number of carbon atoms C_n obtained for each heat source temperature and hydrocarbon family; from left to right: $T_{hi} = 150,\ 250$ and 350 °C.

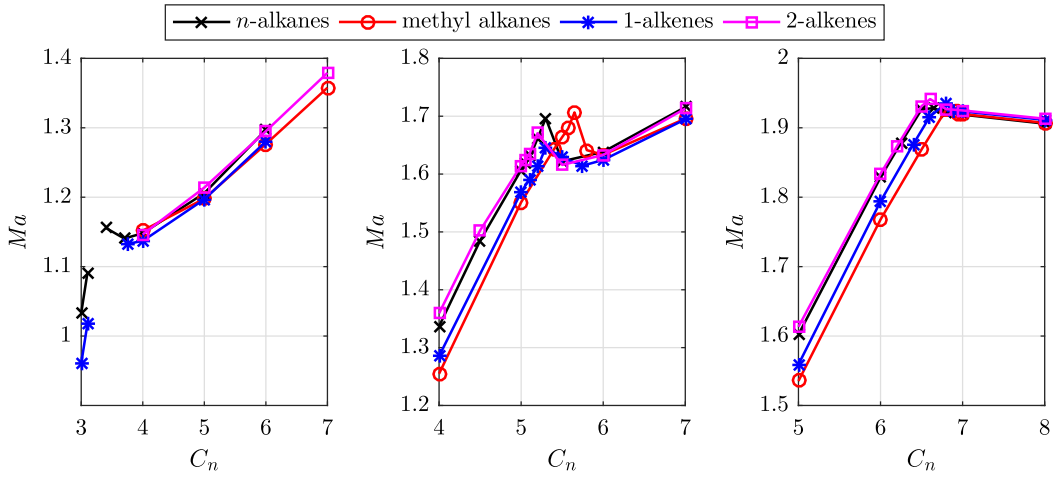

Fig. 16. The rotor inlet Mach number as a function of the number of carbon atoms C_n obtained for each heat-source temperature and hydrocarbon family; from left to right: $T_{hi} = 150,\ 250$ and 350 °C.

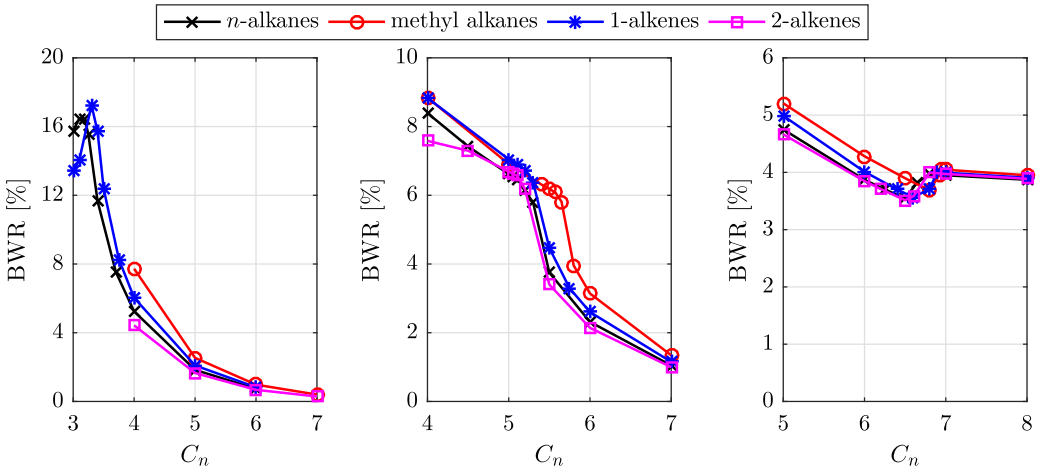

Fig. 17. The back-work ratio (BWR) as a function of the number of carbon atoms C_n obtained for each heat source temperature and hydrocarbon family; from left to right: $T_{hi} = 150,\ 250$ and 350 °C.

increasing pressure ratio and volume ratio rather than being associated to the thermodynamic properties of the gas. This is also confirmed since the difference in the Mach number obtained for each hydrocarbon family is small. Finally, when considering the change in Mach around the optimum power point the change observed is much less significant than that observed for the variation in the volume ratio.

Overall, for all three heat sources the flow conditions at the rotor inlet are supersonic, with Mach numbers approaching $Ma = 2$ for the 350 °C heat source. Therefore suitable radial turbine stator designs would be required that can accelerate the flow to supersonic conditions. This can complicate the turbine design process, but methods to design such stators have been discussed within the literature [82,83].

Alongside the expander modelling, the effect of the molecular complexity of the working fluid on the pump has been investigated by considering the back-work ratio (BWR); this is defined as the ratio of the pump work to the expander work (*i.e.*, $\dot{W}_p/\dot{W}_e$). For this analysis the pump efficiency is assumed constant, which is an oversimplification, but this is presumed to provide a useful insight into the effect of the molecular complexity on the pump performance. The results are presented in Fig. 17.

The results in Fig. 17 clearly show that the BWR reduces as the number of carbon atoms is reduced. This reduction is due to reduction in the condensation pressure as the number of carbon atoms is increased, which in turn reduces the density at the pump inlet and the work required to pump the fluid. This also explains why the BWR flattens off for $C_n > 7$ for the 350 °C heat-source temperature, since the condensation pressure is constrained to 0.25 bar for these cases.

Overall, this preliminary assessment of the expander and pump performance has shown that the optimal cycles from the thermodynamic optimisation typically result in local maxima in both the expander volume ratio and rotor inlet Mach number. Clearly there exists a trade-off between the optimal power output from the system and the complexity and cost of the system components. Therefore future analysis should introduce cost correlations that can translate these design complexities into component development costs.

6. Conclusions

The aim of this paper has been to present a computer-aided molecular design (CAMD) framework for the optimisation of organic Rankine cycle (ORC) power systems based on the molecular-based, group-contribution SAFT-γ Mie equation of state. SAFT-γ Mie has not been previously employed in such a framework. This type of CAMD-ORC framework stands out from conventional modelling approaches in the literature in that it enables the integrated and simultaneous identification of optimal working-fluids, system designs and operational conditions for specific applications. The key aspects of the framework have been presented and validated. In particular, ORC performance calculations completed using SAFT-γ Mie agree very well with calculations performed using NIST REFPROP, and with results from another CAMD-ORC optimisation study available in the literature [54]. A case-study is then considered in order to demonstrate the capabilities of the framework and to determine the optimal hydrocarbon working-fluids and subcritical, non-recuperated ORC systems for waste-heat sources at 150, 250 and 350 °C, each with a heat capacity rate ($\dot{m}c_p$) of 4.2 kW/K. The results suggest that a theoretical optimum fluid, which maximises the power output, should have thermodynamic properties such that the evaporation pressure is maximised and the amount of superheating is minimised. This reduces the latent heat of vaporisation, permitting a better thermal match between the working fluid and heat source. In terms of actual working fluids, simple molecules such as propane and propene are particularly suitable for low-grade (150 °C) heat sources, whilst more complex molecules containing a —CH=CH— double bond are favoured for medium- and higher-grade heat-sources at temperatures between 250 and 350 °C. Specifically, *n*-propane, 2-pentene and 2-hexene are identified as the optimal working-fluids for the three heat-source temperatures, and result in optimal power outputs of 35.2, 136.7 and 219.0 kW, with thermal efficiencies of 9.7, 16.9 and 17.8% respectively. More generally, this study has demonstrated how conventional working-fluid selection studies can be replaced with a more holistic approach. Not only does this streamline the design process, but it also removes subjective and pre-emptive screening criteria and introduces the possibility of identifying the next generation of tailored working-fluids and optimised ORC systems for targeted waste-heat recovery and conversion applications in industrial settings, and beyond.

Moving beyond pure thermodynamic considerations towards complete thermoeconomic evaluations, group-contribution methods for predicting the transport properties of hydrocarbon working fluids have also been evaluated against experimental data, with good agreement. This is an important requirement in the sizing and costing of system components, such as the heat exchangers. Furthermore, an analysis of the expander performance shows that

optimal thermodynamic cycles correspond to high expansion volume ratios. Therefore, a trade-off between thermodynamic performance and component design arises that future CAMD-ORC models must capture through suitable thermoeconomic optimisation. These results are critical in informing the future implementation of thermoeconomic optimisation within the CAMD-ORC framework.

Acknowledgements

This work was supported by the UK Engineering and Physical Sciences Research Council (EPSRC) [grant number EP/P004709/1]. Data supporting this publication can be obtained on request from cep-lab@imperial.ac.uk.

Appendix A. Radial turbine modelling

The rotor inlet blade velocity u is determined by the isentropic velocity ratio ν, where ν is defined as the ratio of the blade velocity to the spouting velocity, and the spouting velocity is a velocity that has the same energy as the isentropic enthalpy drop across the turbine, hence:

$$u = \nu\sqrt{2(h_3 - h_{4s})}. \tag{A.1}$$

The meridional velocity c_m and absolute tangential velocity c_t of the gas at the rotor inlet are then given by the flow coefficient ϕ, and the blade loading coefficient ψ, from which the absolute flow velocity c follows:

$$c_m = \phi u; \tag{A.2}$$

$$c_t = \psi u; \tag{A.3}$$

$$c = \sqrt{c_m^2 + c_t^2}. \tag{A.4}$$

The actual static enthalpy h, and isentropic static enthalpy h_s, follow from an energy balance and an assumed stator isentropic efficiency η_n:

$$h = h_3 - \frac{1}{2}c^2; \tag{A.5}$$

$$h_s = h_3 - \frac{h_3 - h}{\eta_n}. \tag{A.6}$$

Finally, the static pressure P and speed of sound a follow from the equation of state, and the Mach number Ma is determined:

$$P = \mathrm{EoS}(h_s, s_3, \mathrm{fluid}); \tag{A.7}$$

$$a = \mathrm{EoS}(P, h, \mathrm{fluid}); \tag{A.8}$$

$$Ma = \frac{c}{a}. \tag{A.9}$$

The assumptions made for the non-dimensional turbine design parameters are summarised in Table A.1, and these values are based on recommendations made within common turbomachinery textbooks [84].

Table A.1
Turbine design parameters.

ν	ϕ	ψ	η_n
0.7	0.25	0.90	0.9

References

[1] Markides CN. The role of pumped and waste heat technologies in a high-efficiency sustainable energy future for the UK. Appl Therm Eng 2013;53(2):197–209.
[2] Markides CN. Low-concentration solar-power systems based on organic Rankine cycles for distributed-scale applications: overview and further developments. Front Energy Res 2015;3(December):1–16. http://dx.doi.org/10.3389/fenrg.2015.00047.
[3] Chen H, Goswami DY, Stefanakos EK. A review of thermodynamic cycles and working fluids for the conversion of low-grade heat. Renew Sustain Energy Rev 2010;14(9):3059–67. http://dx.doi.org/10.1016/j.rser.2010.07.006.
[4] Hung TC, Shai TY, Wang SK. A review of organic rankine cycles (ORCs) for the recovery of low-grade waste heat. Energy 1997;22(7):661–7. http://dx.doi.org/10.1016/S0360-5442(96)00165-X.
[5] Saleh B, Koglbauer G, Wendland M, Fischer J. Working fluids for low-temperature organic Rankine cycles. Energy 2007;32:1210–21. http://dx.doi.org/10.1016/j.energy.2006.07.001.
[6] He C, Liu C, Gao H, Xie H, Li Y, Wu S, et al. The optimal evaporation temperature and working fluids for subcritical organic Rankine cycle. Energy 2012;38(1):136–43. http://dx.doi.org/10.1016/j.energy.2011.12.022.
[7] Li C, Wang H. Power cycles for waste heat recovery from medium to high temperature flue gas sources – from a view of thermodynamic optimization. Appl Energy 2016;180:707–21. http://dx.doi.org/10.1016/j.apenergy.2016.08.007.
[8] Song J, Gu C-w, Ren X. Parametric design and off-design analysis of organic Rankine cycle (ORC) system. Energy Convers Manage 2016;112:157–65. http://dx.doi.org/10.1016/j.enconman.2015.12.085.
[9] Lecompte S, Ameel B, Ziviani D, Van Den Broek M, De Paepe M. Exergy analysis of zeotropic mixtures as working fluids in organic Rankine cycles. Energy Convers Manage 2014;85:727–39. http://dx.doi.org/10.1016/j.enconman.2014.02.028.
[10] Lu J, Zhang J, Chen S, Pu Y. Analysis of organic Rankine cycles using zeotropic mixtures as working fluids under different restrictive conditions. Energy Convers Manage 2016;126:704–16. http://dx.doi.org/10.1016/j.enconman.2016.08.056.
[11] Oyewunmi OA, Taleb AI, Haslam AJ, Markides CN. An assessment of working-fluid mixtures using SAFT-VR Mie for use in organic Rankine cycle systems for waste-heat recovery. Comput Therm Sci 2014;6:301–16. http://dx.doi.org/10.1615/.2014011116.
[12] Oyewunmi OA, Taleb AI, Haslam AJ, Markides CN. On the use of SAFT-VR Mie for assessing large-glide fluorocarbon working-fluid mixtures in organic Rankine cycles. Appl Energy 2016;163:263–82. http://dx.doi.org/10.1016/j.apenergy.2015.10.040.
[13] Zhou Y, Zhang F, Yu L. Performance analysis of the partial evaporating organic Rankine cycle (PEORC) using zeotropic mixtures. Energy Convers Manage 2016;129:89–99. http://dx.doi.org/10.1016/j.enconman.2016.10.009.
[14] Badr O, Probert SD, O'Callaghan PW. Selecting a working fluid for a Rankine-cycle engine. Appl Energy 1985;21(1):1–42.
[15] Rahbar K, Mahmoud S, Al-Dadah RK, Moazami N, Mirhadizadeh SA. Review of organic Rankine cycle for small-scale applications. Energy Convers Manage 2017;134:135–55. http://dx.doi.org/10.1016/j.enconman.2016.12.023.
[16] Dai X, Shi L, An Q, Qian W. Screening of hydrocarbons as supercritical ORCs working fluids by thermal stability. Energy Convers Manage 2016;126:632–7. http://dx.doi.org/10.1016/j.enconman.2016.08.024.
[17] Lemmon EW, Huber ML, McLinden MO. NIST standard reference database 23: reference fluid thermodynamic and transport properties-REFPROP; 2013.
[18] Drescher U, Brüggemann D. Fluid selection for the organic Rankine cycle (ORC) in biomass power and heat plants. Appl Therm Eng 2007;27(1):223–8. http://dx.doi.org/10.1016/j.applthermaleng.2006.04.024.
[19] Tchanche BF, Papadakis G, Lambrinos G, Frangoudakis A. Fluid selection for a low-temperature solar organic Rankine cycle. Appl Therm Eng 2009;29(11-12):2468–76. http://dx.doi.org/10.1016/j.applthermaleng.2008.12.025.
[20] Schwöbel JAH, Preißinger M, Brüggemann D, Klamt A. High-throughput-screening of working fluids for the organic Rankine cycle (ORC) based on COSMO-RS and thermodynamic process simulations. Ind Eng Chem Res 2017;56:788–98. http://dx.doi.org/10.1021/acs.iecr.6b03857.
[21] Gani R, Brignole EA. Molecular design of solvents for liquid extraction based on UNIFAC. Fluid Phase Equilib 1983;13(C):331–40. http://dx.doi.org/10.1016/0378-3812(83)80104-6.
[22] Bardow A, Steur K, Gross J. Continuous-molecular targeting for integrated solvent and process design. Ind Eng Chem Res 2010;49(6):2834–40. http://dx.doi.org/10.1021/ie901281w.
[23] Stavrou M, Lampe M, Bardow A, Gross J. Continuous molecular targeting computer-aided molecular design (CoMT-CAMD) for simultaneous process and solvent design for CO_2 capture. Ind Eng Chem Res 2014;53(46):18029–41. http://dx.doi.org/10.1021/ie502924h.
[24] Burger J, Papaioannou V, Gopinath S, Jackson G, Galindo A, Adjiman C. A hierarchical method to integrated solvent and process deisgn of physical CO_2 absorption using the SAFT-γ Mie approach. AIChE J 2015;61(10):3249–69. http://dx.doi.org/10.1002/aic. arXiv:arXiv:1402.6991v1.
[25] Gopinath S, Jackson G, Galindo A, Adjiman C. Outer approximation algorithm with physical domain reduction for computer-aided molecular and separation process design. AIChE J 2016;62(9):3484–504. http://dx.doi.org/10.1002/aic. arXiv:arXiv:1402.6991v1.

[26] Gani R, Nielsen B, Fredenslund A. A group contribution approach to computer-aided molecular design. AIChE J 1991;37(9):1318–32. http://dx.doi.org/10.1002/aic.690370905.

[27] Odele O, Macchietto S. Computer aided molecular design: a novel method for optimal solvent selection. Fluid Phase Equilib 1993;82:47–54.

[28] Churi N, Achenie LEK. Novel mathematical programming model for computer aided molecular design. Ind Eng Chem Res 1996;35(96):3788–94. http://dx.doi.org/10.1021/ie9601920.

[29] Joback KG, Reid RC. Estimation of pure-component properties from group-contributions. Chem Eng Commun 1987;57(1-6):233–43. http://dx.doi.org/10.1080/00986448708960487.

[30] Fredenslund A, Jones RL, Prausnitz JM. Group-contribution estimation of activity coefficients in nonideal liquid mixtures. AIChE J 1975;21(6):1086–99. http://dx.doi.org/10.1002/aic.690210607.

[31] Chapman WG, Gubbins KE, Jackson G, Radosz M. SAFT: equation-of-state solution model for associating fluids. Fluid Phase Equilib 1989;52:31–8. http://dx.doi.org/10.1016/0378-3812(89)80308-5.

[32] Chapman WG, Gubbins KE, Jackson G, Radosz M. New reference equation of state for associating liquids. Ind Eng Chem Res 1990;29(8):1709–21. http://dx.doi.org/10.1021/ie00104a021.

[33] Vijande J, Piñeiro MM, Legido JL, Bessières D. Group-contribution method for the molecular parameters of the PC-SAFT equation of state taking into account the proximity effect. Application to nonassociated compounds. Ind Eng Chem Res 2010;49(19):9394–406. http://dx.doi.org/10.1021/ie1002813.

[34] Vijande J, Piñeiro MM, Legido JL. Group-contribution method with proximity effect for PC-SAFT molecular parameters. 2. Application to association parameters: primary alcohols and amines. Ind Eng Chem Res 2014;53(2):909–19. http://dx.doi.org/10.1021/ie4023786.

[35] Tamouza S, Passarello JP, Tobaly P, De Hemptinne JC. Group contribution method with SAFT EOS applied to vapor liquid equilibria of various hydrocarbon series. Fluid Phase Equilib 2004;222-223:67–76. http://dx.doi.org/10.1016/j.fluid.2004.06.038.

[36] Tamouza S, Passarello JP, Tobaly P, De Hemptinne JC. Application to binary mixtures of a group contribution SAFT EOS (GC-SAFT). Fluid Phase Equilib 2005;228-229:409–19. http://dx.doi.org/10.1016/j.fluid.2004.10.003.

[37] Nguyen-Huynh D, Passarello J-P, Tobaly P, de Hemptinne J-C. Modeling phase equilibria of asymmetric mixtures using a group-contribution SAFT (GC-SAFT) with a k_{ij} correlation method based on London's theory. 1. Application to CO_2 + n-alkane, methane + n-alkane, and ethane + n-alkane systems. Ind Eng Chem Res 2008;47(22):8847–58. http://dx.doi.org/10.1021/ie071643r.

[38] Tihic A, Kontogeorgis GM, von Solms N, Michelsen ML, Constantinou L. A predictive group-contribution simplified PC-SAFT equation of state: application to polymer systems. Ind Eng Chem Res 2008;47:5092–101. http://dx.doi.org/10.1021/ie0710768.

[39] Nguyen Thi TX, Tamouza S, Tobaly P, Passarello JP, De Hemptinne JC. Application of group contribution SAFT equation of state (GC-SAFT) to model phase behaviour of light and heavy esters. Fluid Phase Equilib 2005;238(2):254–61. http://dx.doi.org/10.1016/j.fluid.2005.10.009.

[40] Emami FS, Vahid A, Elliott JR, Feyzi F. Group contribution prediction of vapor pressure with SAFT, perturbed-chain statistical associating fluid theory, and Elliott-Suresh-Donohue equations of state. Ind Eng Chem Res 2008;47:8401–11. http://dx.doi.org/10.1021/ie800329r.

[41] Lymperiadis A, Adjiman CS, Galindo A, Jackson G. A group contribution method for associating chain molecules based on the statistical associating fluid theory (SAFT-γ). J Chem Phys 2007;127(23):234903. http://dx.doi.org/10.1063/1.2813894.

[42] Lymperiadis A, Adjiman CS, Jackson G, Galindo A. A generalisation of the SAFT-γ group contribution method for groups comprising multiple spherical segments. Fluid Phase Equilib 2008;274(1-2):85–104. http://dx.doi.org/10.1016/j.fluid.2008.08.005.

[43] Peng Y, Goff KD, dos Ramos MC, McCabe C. Developing a predictive group-contribution-based SAFT-VR equation of state. Fluid Phase Equilib 2009;277(2):131–44. http://dx.doi.org/10.1016/j.fluid.2008.11.008.

[44] Papaioannou V, Lafitte T, Avendaño C, Adjiman CS, Jackson G, Müller EA, et al. Group contribution methodology based on the statistical associating fluid theory for heteronuclear molecules formed from Mie segments. J Chem Phys 2014;140(5):1–29. http://dx.doi.org/10.1063/1.4851455.

[45] Papadopoulos AI, Stijepovic M, Linke P. On the systematic design and selection of optimal working fluids for organic Rankine cycles. Appl Therm Eng 2010;30(6–7):760–9. http://dx.doi.org/10.1016/j.applthermaleng.2009.12.006.

[46] Papadopoulos AI, Stijepovic M, Linke P, Seferlis P, Voutetakis S. Toward optimum working fluid mixtures for organic Rankine cycles using molecular design and sensitivity analysis. Ind Eng Chem Res 2013;52(34):12116–33. http://dx.doi.org/10.1021/ie400968j.

[47] Brignoli R, Brown JS. Organic Rankine cycle model for well-described and not-so-well-described working fluids. Energy 2015;86:93–104. http://dx.doi.org/10.1016/j.energy.2015.03.119.

[48] Palma-Flores O, Flores-Tlacuahuac A, Canseco-Melchorb G. Simultaneous molecular and process design for waste heat recovery. Energy 2016;99:32–47. http://dx.doi.org/10.1016/j.energy.2016.01.024.

[49] Su W, Zhao L, Deng S. Developing a performance evaluation model of organic Rankine cycle for working fluids based on the group contribution method. Energy Convers Manage 2017;132:307–15. http://dx.doi.org/10.1016/j.enconman.2016.11.040.

[50] Gross J, Sadowski G. Perturbed-chain SAFT: an equation of state based on a perturbation theory for chain molecules. Ind Eng Chem Res 2001;40(4):1244–60. http://dx.doi.org/10.1021/ie0003887.

[51] Gross J, Sadowski G. Modeling polymer systems using the perturbed-chain statistical associating fluid theory equation of state. Ind Eng Chem Res 2002;41(5):1084–93. http://dx.doi.org/10.1021/ie010449g.

[52] Lampe M, Stavrou M, Bucker HM, Gross J, Bardow A. Simultaneous optimization of working fluid and process for organic rankine cycles using PC-SAFT. Ind Eng Chem Res 2014;53(21):8821–30. http://dx.doi.org/10.1021/ie5006542.

[53] Lampe M, Stavrou M, Schilling J, Sauer E, Gross J, Bardow A. Computer-aided molecular design in the continuous-molecular targeting framework using group-contribution PC-SAFT. Comput Chem Eng 2015;81:278–87. http://dx.doi.org/10.1016/j.compchemeng.2015.04.008.

[54] Schilling J, Lampe M, Gross J, Bardow A. 1-stage CoMT-CAMD: an approach for integrated design of ORC process and working fluid using PC-SAFT. Chem Eng Sci 2017;159:217–30. http://dx.doi.org/10.1016/j.ces.2016.04.048.

[55] Lafitte T, Apostolakou A, Avendaño C, Galindo A, Adjiman CS, Müller EA, et al. Accurate statistical associating fluid theory for chain molecules formed from Mie segments. J. Chem. Phys. 139(15) http://dx.doi.org/10.1063/1.4819786.

[56] Dufal S, Papaioannou V, Sadeqzadeh M, Pogiatzis T, Chremos A, Adjiman CS, et al. Prediction of thermodynamic properties and phase behavior of fluids and mixtures with the SAFT-γ Mie group-contribution equation of state. J Chem Eng Data 2014;59(10):3272–88. http://dx.doi.org/10.1021/je500248h.

[57] Papaioannou V, Calado F, Lafitte T, Dufal S, Sadeqzadeh M, Jackson G, et al. Application of the SAFT-γ Mie group contribution equation of state to fluids of relevance to the oil and gas industry. Fluid Phase Equilib 2015;416:104–19. http://dx.doi.org/10.1016/j.fluid.2015.12.041.

[58] Oyewunmi OA, Haslam AJ, Markides CN. Towards the computer-aided molecular design of organic Rankine cycle systems with advanced fluid theories. In: SusTEM 2015 international conference, 7–8th July, Newcastle upon Tyne, UK; 2013.

[59] Process Systems Enterprise Ltd., gPROMS. <http://www.psenterprise.com>.

[60] Invernizzi CM. Closed power cycles. Lecture notes in energy, vol. 11. London: Springer-Verlag; 2013. http://dx.doi.org/10.1007/978-1-4471-5140-1.

[61] Vaja I, Gambarotta A. Internal combustion engine (ICE) bottoming with organic Rankine cycles (ORCs). Energy 2010;35(2):1084–93. http://dx.doi.org/10.1016/j.energy.2009.06.001.

[62] Oyewunmi OA, Markides CN. Thermo-economic and heat transfer optimization of working-fluid mixtures in a low-temperature organic rankine cycle system. Energies 2016;9(6):448. http://dx.doi.org/10.3390/en9060448. , <http://www.mdpi.com/1996-1073/9/6/448>.

[63] Poling BE, Prausnitz JM, John Paul O, Reid RC. The properties of gases and liquids, vol. 5. New York: McGraw-Hill; 2001.

[64] Constantinou L, Gani R. New group contribution method for estimating properties of pure compounds. AIChE J 1994;40(10):1697–710. http://dx.doi.org/10.1002/aic.690401011.

[65] Ambrose D, Walton J. Vapour pressures up to their critical temperatures of normal alkanes and 1-alkanols. Pure Appl Chem 1989;61(8):1395–403.

[66] Pitzer KS, Lippmann DZ, Curl RF, Huggins CM, Petersen DE, volumetric The, et al. vapor pressure and entropy of vaporization. J Am Chem Soc 1955;77(13):3433–40. http://dx.doi.org/10.1021/ja01618a002. arXiv:http://dx.doi.org/10.1021/ja01618a002.

[67] Sastri S, Rao K. A new group contribution method for predicting viscosity of organic liquids. Chem Eng J 1992;50(1):9–25. http://dx.doi.org/10.1016/0300-9467(92)80002-R, <http://www.sciencedirect.com/science/article/pii/030094679280002R>.

[68] Reichenberg D. The viscosity of organic vapors at low pressures. DSC Rep 1971;11:484.

[69] Reichenberg D. The estimation of the viscosities of gases and gas mixtures. In: Symposium on transport properties of fluids and fluid mixtures, their measurement, estimation, correlation and use, East Kilbride, Glasgow, Scotland; 1979.

[70] Reichenberg D. New methods for the estimation of the viscosity coefficients of pure gases at moderate pressures (with particular reference to organic vapors). AIChE J 1975;21(1):181–3. http://dx.doi.org/10.1002/aic.690210130, <http://dx.doi.org/10.1002/aic.690210130>.

[71] Reichenberg D. New simplified methods for the estimation of the viscosities of gas mixtures at moderate pressures. NASA STI/Recon Technical Report N 77.

[72] Chung TH, Lee LL, Starling KE. Applications of kinetic gas theories and multiparameter correlation for prediction of dilute gas viscosity and thermal conductivity. Ind Eng Chem Fund 1984;23(1):8–13. http://dx.doi.org/10.1021/i100013a002. arXiv:http://dx.doi.org/10.1021/i100013a002.

[73] Chung TH, Ajlan M, Lee LL, Starling KE. Generalized multiparameter correlation for nonpolar and polar fluid transport properties. Ind Eng Chem Res 1988;27(4):671–9. http://dx.doi.org/10.1021/ie00076a024. arXiv:http://dx.doi.org/10.1021/ie00076a024.

[74] Latini G, Pacetti M. Liquid thermal conductivity, correlations and estimations. Bull Int Inst Refrig 1977;57(6):1446–73.

[75] Baroncini C, Di Filippo P, Latini G, Pacetti M. An improved correlation for the calculation of liquid thermal conductivity. Int J Thermophys 1980;1(2):159–75. http://dx.doi.org/10.1007/BF00504518.

[76] Baroncini C, Di Filippo P, Latini G, Pacetti M. Organic liquid thermal conductivity: a prediction method in the reduced temperature range 0.3 to 0.8. Int J Thermophys 1981;2(1):21–38. http://dx.doi.org/10.1007/BF00503572.
[77] Sastri S, Rao K. Quick estimating for thermal conductivity. Chem Eng 1993;100(8):106.
[78] Svehla RA. Estimated viscosities and thermal conductivities of gases at high temperatures, Tech. rep. National Aeronautics and Space Administration. Lewis Research Center, Cleveland; 1962.
[79] Stiel LI, Thodos G. The thermal conductivity of nonpolar substances in the dense gaseous and liquid regions. AIChE J 1964;10(1):26–30. http://dx.doi.org/10.1002/aic.690100114.
[80] Sastri S, Rao K. A simple method to predict surface tension of organic liquids. Chem Eng J Biochem Eng J 1995;59(2):181–6. http://dx.doi.org/10.1016/0923-0467(94)02946-6, <http://www.sciencedirect.com/science/article/pii/0923046794029466>.
[81] Colonna P, Casati E, Trapp C, Mathijssen T, Larjola J, Turunen-Saaresti T, et al. Organic Rankine cycle power systems: from the concept to current technology, applications, and an outlook to the future. J. Eng. Gas Turb Power 137(10). http://dx.doi.org/10.1115/1.4029884.
[82] Pasquale D, Ghidoni A, Rebay S. Shape optimization of an organic Rankine cycle radial turbine nozzle. J Eng Gas Turbines Power 2013;135(4):1–13. http://dx.doi.org/10.1115/1.4023118.
[83] Pini M, Persico G, Pasquale D, Rebay S. Adjoint method for shape optimization in real-gas flow applications. J Eng Gas Turbines Power 2015;137(3):032604. http://dx.doi.org/10.1115/1.4028495.
[84] Moustapha H, Zelesky MF, Baines NC, Japiske D. Axial and radial turbines. Concepts ETI, Inc.; 2003.